Michelle Hechenbichler, Albert Prause, Michael Gradzielski, André Laschewsky

Thermoresponsive self-assembly of twofold fluorescently labeled block copolymers in aqueous solution and microemulsions

Citation details
Hechenbichler, M., Prause, A., Gradzielski, M., & Laschewsky, A. (2021). Thermoresponsive Self-Assembly of Twofold Fluorescently Labeled Block Copolymers in Aqueous Solution and Microemulsions. In Langmuir (Vol. 38, Issue 17, pp. 5166–5182). American Chemical Society (ACS). https://doi.org/10.1021/acs.langmuir.1c02318.

Thermo-responsive Self-assembly of Two-fold Fluorescently Labelled Block Copolymers in Aqueous Solution and Microemulsions.

Michelle Hechenbichler [a], *Albert Prause* [b], *Michael Gradzielski* [b,*] *and André Laschewsky* [a,c] *

[a] Institut für Chemie, Universität Potsdam, Karl-Liebknecht-Straße 24-25, 14476, Potsdam-Golm/Germany

[b] Stranski-Laboratorium für Physikalische und Theoretische Chemie, FG Physical Chemistry/ Molecular Material Science Institute of Chemistry, Technische Universität Berlin, Straße des 17. Juni 124, 10623, Berlin/Germany

[c] Fraunhofer Institute of Applied Polymer Research IAP, Fraunhofer Institute, Geiselbergstr. 69, 14476, Potsdam-Golm/Germany

KEYWORDS: watersoluble polymer, associative polymer, amphiphile, thermo-responsive, self-assembly, fluorescence label, FRET.

ABSTRACT

A nonionic double hydrophilic block copolymer with a long permanently hydrophilic and a small thermo-responsive block is synthesized by reversible addition fragmentation chain transfer

polymerization (RAFT). Employing a specifically designed chain transfer agent, the polymer is functionalized with complementary end groups which are suited for Förster resonance energy transfer (FRET). The end group attached to the permanently hydrophilic block of poly(*N*,*N*–dimethylacrylamide) pDMAm is designed as permanently hydrophobic segment ('sticker') comprising a long alkyl chain and the 4-aminonaphthalimide fluorophore. The other end attached to the thermo-responsive block of poly(*N*–isopropylacrylamide) pNiPAm incorporates a coumarin fluorophore. The temperature-dependent self-assembly of the two-fold fluorescently labelled copolymer is studied in pure aqueous solution as well as in an o/w microemulsion by several techniques including turbidimetry, dynamic light scattering (DLS), and fluorescence spectroscopy. It is compared to the behaviors of the analogous two-fold labelled pDMAm and pNiPAm homopolymer references. The findings indicate that the block copolymer behaves as polymeric surfactant at low temperatures, with one relatively small hydrophobic end block and an extended hydrophilic chain forming 'hairy micelles'. At elevated temperatures above the LCST phase transition of the pNiPAm block, however, the copolymer behaves as associative telechelic polymer with two non-symmetrical hydrophobic end blocks, which do not mix. Thus, instead of a network of bridged 'flower micelles', large dynamic aggregates are formed. These are connected alternatingly by the original micellar cores as well as by clusters of the collapsed pNiPAm blocks. This type of structure is even more favored in the w/o microemulsion than in pure aqueous solution, as the microemulsion droplets constitute an attractive anchoring point for the hydrophobic dodecyl sticker, but not for the collapsed pNiPAm chains.

.

INTRODUCTION

Because of the inherently reduced mixing entropy and the resulting strong tendency for (micro)phase separation, as well as by virtue of the substantially increased number of molecular variables in comparison to low molar mass surfactants, polymeric amphiphiles give rise to a plethora of self-organized structures in selective solvents, in particular in aqueous media.[1-7] Two major polymer classes are conveniently distinguished according to the origin of the amphiphilic character. On the one hand, the constitutional monomer units (CRU), or at least short monomer sequences, are inherently amphiphilic, as e.g. in the so-called polysoaps.[7-9] On the other hand, amphiphilicity can result from the overall macromolecular architecture that combines individual hydrophobic and hydrophilic blocks, as e.g. in amphiphilic graft and block copolymers ("macro surfactants").[1, 4, 7] While formerly, amphiphilic block copolymers were restricted to a small number of practical systems, the advent of the Reversible Deactivation Radical Polymerization (RDRP) methods has diversified the synthesis of block copolymers exceedingly, and concomitantly the investigation and use of the latter copolymer class enormously during the past two decades.[10-14] A particular aspect of amphiphilic block copolymers is the relative ease of implementing responsive (also called 'smart' or 'intelligent') amphiphilic systems, which react to a small change of a trigger parameter with important changes of their self-assembly behavior, and thus of their properties.[14-17] Arguably, the most explored trigger is a temperature change, as it is non-invasive and the induced changes are fully reversible in many cases, thus enabling repeated switching of such systems. In aqueous systems, thermo-responsive polymers exploit typically the crossing of a lower consolute boundary, and are characterized by a lower critical solution temperature (LCST). The best-known and most intensely studied example is poly(*N*-isopropylacrylamide) pNiPAm.[18-24] Importantly, it exhibits LCST-behavior of the non-Flory-Huggins type ('Type II' behavior),[25]

reducing substantially the sensitivity of its transition temperature to variations in physical (such as concentration) as well as molecular parameters (such as molar mass). In consequence, pNiPAm has been frequently employed as versatile component in thermo-responsive 'smart' amphiphiles, acting likewise as switchable hydrophobic or switchable hydrophilic block, in dependence on the overall molecular architecture.[26, 27] Up to now, studies have been mostly focused on AB diblock and symmetrical ABA and BAB triblock copolymer systems.[16, 28] 'A' and 'B', respectively, signify the operative hydrophilic and hydrophobic blocks, notwithstanding the use of pNiPAm in more complex architectures such as non-symmetrical triblock,[27, 29, 30] so-called 'schizophrenic',[31, 32] or 'molecular bottlebrush' copolymers.[33, 34] The majority of studies deal with polymers, in which pNiPAm acts as switchable hydrophilic block (A*) in combination with permanently hydrophobic B blocks, or in reverse, as switchable hydrophobic block (B*) in combination with permanently hydrophilic A blocks. Amidst these architectures, symmetrical triblock copolymers of the type B*AB* found special interest as 'smart" associative thickeners,[35-38] in which the amphiphilic character and thus, the aggregation driven modification of rheology can be implemented by a simple temperature stimulus.

With this background, we started recently to explore thermo-responsive amphiphilic block polymers with a non-conventional structure. Specifically, we explore non-symmetrical architectures BAB*, in which a long permanently hydrophilic inner A block is framed on one end by a short permanently hydrophobic end group B ('hydrophobic sticker'), and on the other end by a responsive, conditionally hydrophobic end block B*, which exploits an LCST transition (Scheme 1). Instead of implementing simple 'on-off' systems by rendering a double hydrophilic A*AA* system into an amphiphilic and associative B*AB* system, we aim via this design at 'smart' systems, that switch between a classical surfactant-like BAA* type state and a BAB* triblock

system that behaves as rheology modifier (Scheme 1a). In this way, we aim at promoting systems which transform from isolated ‘hairy micelle’-like assemblies, which produce low viscosity solutions, into 'flower micelle'-like micellar assemblies, which are capable of network formation, thus acting as associative thickeners (Scheme 1b).[39, 40] In such 'hairy micelles', a relatively small hydrophobic core formed by the hydrophobic blocks is surrounded by an extended hydrophilic corona formed by dangling hydrophilic blocks. In contrast in 'flower micelles', the hydrophilic corona is more compact as most of the hydrophilic blocks assume a looped conformation, because the hydrophobic blocks of the individual copolymer reside predominantly in the same micellar core.[2]

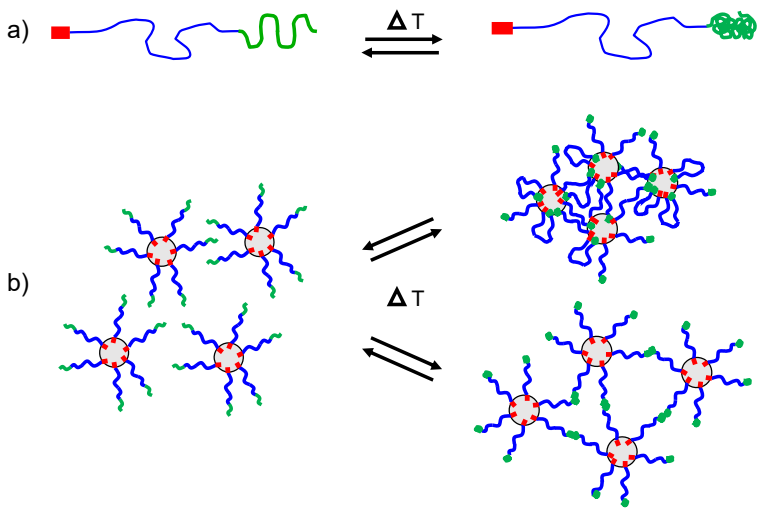

Scheme 1. a) Idealized architecture of an amphiphilic BAB*-type block copolymer consisting of a long hydrophilic central block (A, in blue), capped by one short permanently hydrophobic end group (B, in red) and one thermo-responsive end block (B*, in green); b) model for the temperature-triggered switching of such polymers between isolated hairy micelles (left) and networks of either interconnected flower-like micelles (upper right) or interconnected hairy micelles (lower right).

Due to their particular structure, we may assume that the permanently hydrophobic sticker end B of the copolymers enables their hydrophobic association in the BAA* state into large spherical hairy micelles with small cores that are dynamically equilibrated.[41, 42] For the aggregates formed in the BAB* state, the scenario is a priori less clear after switching the character of the thermo-responsive block from hydrophilic to water-insoluble (Scheme 1b). If the B and B* blocks are sufficiently compatible, one will expect the transformation of the hairy into standard flower micelles (Scheme 1b, upper right). If, however, the B and B* blocks are sufficiently incompatible, additional separate hydrophobic micro domains will be formed by the collapsed B* blocks which coexist with the micellar cores made of the B ends (Scheme 1b, lower right). Both scenarios allow for network formation, and consequently, for implementing enhanced viscosity or inducing gelation. However, the network properties are expected to differ markedly in these two scenarios. For instance, the latter scenario (Scheme 1b, lower right) should markedly increase the average distance between the micellar cores in the network, thus enabling percolation of the aggregates at a much lower polymer concentration. Also, one can speculate whether the formation of separate microdomains of the collapsed B* block can be favored, when o/w microemulsions are used instead of pure water as medium. In fact, rheology control of microemulsions is of great practical importance.[43] In this case, the sticker blocks B would insert into the oil droplets, while the collapsed B* blocks stay out and form separate microdomains, which act as a second population of crosslinking sites. This scenario shows structural similarities to multicompartment micellar hydrogels.[44]

To shed more light onto the aggregation behavior of such BAA*/BAB* systems, we designed the thermo-responsive diblock copolymer **pDMAm−b−NiPAm*** (Figure 1). This polymer is

α,ω–unsymmetrically functionalized with complementary fluorophores suited for Förster resonance energy transfer (FRET).[45] The efficiency of the FRET process depends sensitively on the average distance of the fluorophore donor-acceptor pair at the nm scale. Therefore, appropriately FRET labelled amphiphiles enable the differentiation between aggregates of diverse structures, if these are correlated with the distance of the specific positions of the donor and acceptor groups within the polymers.[46-48] Most of the previous FRET-based studies on the aggregation of amphiphilic polymers have used pairs of donor- and acceptor-labelled polymers (often without defined positions of the fluorophores within a given polymer).[47-58] Yet, the investigation of the scenarios in Scheme 1b requires the incorporation of both donor- and acceptor group into well-defined positions, which preferentially are as distant as possible within the same block copolymer. This has been done rarely up to now.[59-64] Taking the optimal layer substructure of surfactants into account,[65] we thus incorporated a naphthalimide fluorophore as FRET acceptor at the joint of the permanently hydrophobic sticker group and the permanently hydrophilic block, while a coumarin fluorophore was used for capping the thermo-responsive block, thus placing the FRET donor at the opposite polymer terminus (Figure 1). If the collapse of the A* block results in the transformation of the hairy into flower micelles (Scheme 1b, upper part), the FRET efficiency will strongly increase after the temperature-induced transition. If, however, separate microdomains are formed (Scheme 1b, lower part), the collapse of the responsive block will hardly affect the FRET efficiency.

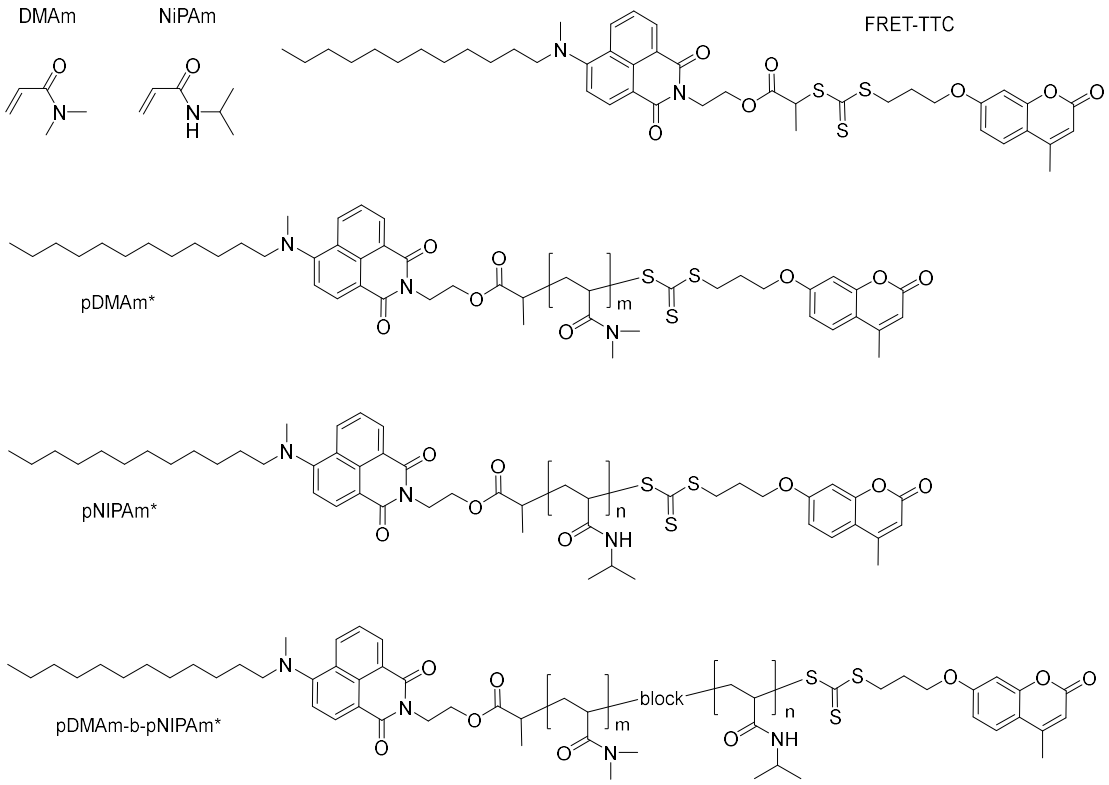

Figure 1. Chemical structures of the monomers (**DMAm** and **NiPAm**) and chain transfer agent (**FRET−TTC**) used, and of the polymers synthesized (**pDMAm***, **pNiPAm***, and **pDMAm−b−pNiPAm***).

For the thermo-responsive AA*/AB* diblock fragment within the target structure, we used the well-established combination of permanently hydrophilic non-ionic poly(*N*,*N*–dimethyl-acrylamide) pDMAm and thermo-responsive poly(*N*-isopropylacrylamide) pNiAm.[29, 66-70] The polymer was synthesized by two successive RAFT polymerizations. The precise positioning of the FRET donor-acceptor pair in the macromolecules was achieved by employing a dually fluorophore-tagged trithiocarbonate, namely **FRET−TTC** (Figure 1), as RAFT chain transfer agent.[12, 71] Within **FRET−TTC**, the acceptor dye is part of the re-initiating so-called 'R-group',

and the donor dye is part of the deactivating so-called 'Z-group'. The unusual FRET pair based on a naphthalimide and a coumarin fluorophore[72] was chosen to cope with some boundary conditions which are to be respected in our specific case. These comprise, *e.g.*, relatively small fluorophore size, inertness in free radical polymerization and the exclusion of potential electrostatic interactions (thus e.g. excluding the popular fluorescein/rhodamine pairs), as well as good tolerance to quencher groups such as trithiocarbonates,[61] and rather high hydrophobicity of the acceptor but low hydrophobicity of the donor dye (thus e.g. excluding the popular pairs of hydrocarbon fluorophores such as naphthalene/anthracene/phenantrene/pyrene). Moreover, the particular 4-amino-substituted naphthalimide fluorophore shows a pronounced solvatochromism,[73, 74] which may possibly provide additional clues about the changes of the polymer's aggregation behavior.[75]

The dually fluorophore-tagged copolymer **pDMAm−b−pNiPAm*** was studied with respect to its thermo-responsive behavior by temperature-dependent turbidimetry, dynamic light scattering (DLS), small angle X-ray scattering (SAXS), and fluorescence behavior. The analogously dually fluorophore-tagged homopolymers, **pDMAm*** and **pNiPAm*** (Figure 1), were also synthesized and studied as references.

EXPERIMENTAL ‘SECTION

Materials

N–methyldodecylamine was prepared from methylamine hydrochloride (≥ 98 %, Fluka) and 1–bromododecane (≥ 95 %, Fluka) according to the literature.[76] Reagents allylbromide (99 % stabilized with propylene oxide, Sigma Aldrich), 2–bromopropionyl bromide (97 %, Sigma

Aldrich), carbon disulfide (≥ 99.9 %, Merck), 4–chloro-1,8–naphthalic anhydride (95.0 %, Fluka), 7–hydroxy-4–methylcoumarin (97 %, Acros Organics), thioacetic acid (≥ 98 %, Merck), triethylamine (≥ 99.5 %, Roth) were used as received. Ethanolamine (≥ 99.0 %, Sigma Aldrich) was distilled prior to use. Tetradecyldimethylamine–*N*–oxide (TDMAO, Ammonyx MO, Stepan) was freeze-dried, recrystallized in acetone and dried under reduced pressure. *N*–isopropylacrylamide (NIPAm, 97 %, Merck) was crystallized from *n*–heptane prior to use. *N*,*N*–dimethylacrylamide (DMAm, ≥ 99.0 %, stabilized with MEHQ, TCI) was distilled prior to use to remove the inhibitor. 2,2′–azobis(2–methylpropionitrile) (AIBN, 98 %, Merck) was crystallized from n-hexane prior to use. 1,1′–azobis(cyclohexanecarbonitrile) (V40, 98 %, Merck) was crystallized from chloroform prior to use. Solvents benzene (99.5 %, Roth), chloroform (≥ 99.5 % stabilized with amylene, Th.Geyer), chloroform–d (99.8 atom% D, Armar Chemicals), *n*–decane (≥ 98 %, Fluka), deuterium oxide (99.8 atom% D, Armar Chemicals), dichloromethane, (≥ 99.8 % stabilized with amylene, Th.Geyer), dichloromethane (≥ 99.5 %, Roth), diethylether (≥ 95.5 %, Th.Geyer), *N*,*N*–dimethylformamide (> 99 %, Acros Organics), ethanol (absolute, Merck), ethyl acetate (99.9 %, VWR), *n*–hexane (≥ 95.0 %, Chemsolute/Th.Geyer), 1–pentanol (≥ 99 %, Sigma Aldrich), petrol ether (boiling range 60-80 °C, analytical grade, Chemsolute/Th.Geyer), and tetrahydrofuran (≥ 99.5 % stabilized with BHT, Acros) were used as received. For polymerizations, tetrahydrofuran was additionally distilled prior to use to remove inhibitor. For spectroscopic studies, tetrahydrofuran and dichloromethane were additionally distilled and stored over $MgSO_4$ prior to use.

1 M Aqueous hydrochloric acid (Th.Geyer), concentrated hydrochloric acid (Chemsolute/Th.Geyer), magnesium sulfate, (anhydrous, Applichem, Darmstadt/Germany),

potassium carbonate (anhydrous, ≥ 99 %, Roth), potassium iodide (≥ 99.99 %, Sigma Aldrich), sodium chloride (≥ 99.0 %, Th.Geyer), and sodium hydroxide (≥ 98.8 %, Chemsolute) were used as received. Deionized (DI) water was used for synthesis. For turbidimetry, DLS and fluorescence studies, ultapure water (resistivity 18 MΩ·cm^{-1}) was used, obtained by post-treating DI water by a Millipore Milli-Q Plus water purification system (Merck Millipore, Darmstadt/Germany). The nonionic microemulsion was prepared by dissolving precise amounts of TDMAO (190.0 mmol·L^{-1}) and of decane (57.3 mmol·L^{-1}) in ultapure water, which are known to form spherical microemulsion droplets of about 3.1 nm in radius.[77] Silica gel 60 (0.063-0.200 mm, 230-400 mesh ASTM, Merck) was used as stationary phase for column chromatography.

Synthesis of 4−(*N*'−dodecyl−*N*'−methyl)amino)-*N*−2−hydroxyethyl-1,8−naphthalimide (**2**)

Adapting a procedure from the literature,[73] 4–chloro-1,8–naphthalic anhydride (10.00 g, 42.99 mmol) and *N*-methyldodecylamine (17.14 g, 85.98 mmol, 2.00 eq.) in pentanol (100 mL) were refluxed for 24 h with stirring under argon atmosphere. After cooling to room temperature, the crystals formed were filtered off, washed with ethanol, and crystallized twice from ethanol before purification by column chromatography (silica gel, eluent petrol ether/ethyl acetate (5:1 (v/v), R_f= 0.16). Final crystallization from petrol ether/ethyl acetate (5:1 (v/v)) yielded 4.76 g (12.0 mmol, 28 %) of 4−(*N*'−dodecyl-*N*'−methyl)amino-1,8−naphthalic anhydride **1** as orange powder.

^{1}H-NMR (400 MHz in $CDCl_3$, δ in ppm): δ = 0.87 (t, *J* = 6.9 Hz, 3H, CH_2-C$\underline{H}_3$), 1.24-1.29 (m, 18H, (C$\underline{H}_2$)$_9$-CH_3), 1.76 (br. tt, J^1= J^2= 7.3 Hz, 2H, N-CH_2-C$\underline{H}_2$), 3.11 (s, 3H, N-C$\underline{H}_3$), 3.39 (br. t, *J* = 7.6 Hz, 2H, N-C$\underline{H}_2$), 7.14 (d, *J* = 8.4 Hz, 1H, ArH^3), 7.67 (dd, J^1= J^2= 7.3 Hz, 1H, ArH^6), 8.45

(dd, J = 1.1 Hz, J = 8.2 Hz, 1H, ArH^2), 8.47 (d, J = 8.2 Hz, 1H, ArH^7), 8.57 (dd, J = 1.1 Hz, J = 7.4 Hz, 1H, ArH^5).

In the next step, 4−(*N*′−dodecyl-*N*′−methyl)amino-1,8−naphthalic anhydride **1** (1.59 g, 4.02 mmol) and ethanolamine (0.84 mL, 0.86 g, 14.03 mmol, 1.3 eq) were refluxed in ethanol (100 mL) for 26 h. After cooling to room temperature, the formed yellow crystals were filtered off. Concentration of the filtrate in the heat and subsequent cooling produced a second crop of crystals. Yield: 1.45 g (3.31 mmol, 82 %) of 4–(*N*′−dodecyl−*N*′−methyl)amino)-*N*−2−hydroxyethyl-1,8−naphthalimide **2**.

^{1}H-NMR (400 MHz in $CDCl_3$, δ in ppm): δ = 0.87 (t, J = 6.9 Hz, 3H, CH_2-C$\underline{H}_3$), 1.24-1.29 (m, 18H, (C$\underline{H}_2$)$_9$-CH_3), 1.74 (br. tt, J^1 = J^2 = 7.0 Hz, 2H, N-CH_2-C$\underline{H}_2$), 3.07 (s, 3H, N-C$\underline{H}_3$), 3.33 (br. t, J = 7.6 Hz, 2H, N-C$\underline{H}_2$), 3.97 (t, J = 5.1 Hz, 2H, -N-C$\underline{H}_2$-O), 4.46 (t, J = 5.2 Hz, 2H, O-C$\underline{H}_2$-), 7.15 (d, J = 8.4 Hz, 1H, ArH^3), 7.66 (dd, J = 7.3 Hz, J = 8.4 Hz, 1H, ArH^6), 8.42 (dd, J = 1.1 Hz, J = 8.5 Hz, 1H, ArH^2), 8.48 (d, J = 8.2 Hz, 1H, ArH^7), 8.58 (dd, J = 1.1 Hz, J = 7.3 Hz, 1H, ArH^5). (see Figure S1)

Synthesis of 4−(*N*′−dodecyl−*N*′−methyl)amino)-1,3-dioxo-1H-benzo[de]isoquinolin-2(3H)−yl)-ethyl 2-bromopropanoate (**3**)

2−Bromopropionyl bromide (0.40 mL, 0.82 g, 3.82 mmol, 1.15 eq.) was added dropwise to a solution of 4–(*N*′−dodecyl−*N*′−methyl)amino)-*N*−2−hydroxyethyl-1,8−naphthalimide **2** (1.45 g, 3.31 mmol) and triethylamine (0.52 mL, 0.38 g, 3.77 mmol 1.14 eq.) in dry CH_2Cl_2 (40 mL), while cooling to 0 °C. After 1 d, more triethylamine (0.52 mL, 0.38 g, 3.77 mmol 1.14 eq.) and 2−bromopropionyl bromide (0.40 mL, 0.82 g, 3.82 mmol, 1.15 eq.) were added, maintaining the temperature at 0 °C. After 1.5 h, the reaction was complete according to thin layer chromatography

(TLC, eluent petrol ether/ethyl acetate 5v:1v). After cooling and dilution by more CH_2Cl_2 (35 mL), the organic phase was separated, washed successively with water (100 mL), 1 M HCl (2 × 50 mL), saturated $NaHCO_3$-solution (50 mL) and brine (50 mL), dried over $MgSO_4$, and the solvent removed under reduced pressure. The orange residue is purified by column chromatography (gradient eluent: petrol ether/ethyl acetate 10:1 (v/v) increasing to 5:1 (v/v)). The thus obtained intermediate 4−(*N*'−dodecyl−*N*'−methyl)amino)-1,3-dioxo-1H-benzo[de]isoquinolin-2(3H)-yl)ethyl-2−bromopropanoate **3** was used without further purification. Yield: 1.50 g (2.62 mmol, 79 %). (see Figure S2)

^{1}H-NMR (400 MHz in $CDCl_3$, δ in ppm): δ = 0.87 (t, *J* = 6.9 Hz, 3H, CH_2-C$\underline{H}_3$), 1.24-1.29 (m, 18H, (C$\underline{H}_2$)$_9$-CH_3), 1.74 (br. tt, $J^1 = J^2 = 7.0$ Hz, 2H, N-CH_2-C$\underline{H}_2$), 1.80 (d, *J* = 7.0 Hz, 3H, CH-C$\underline{H}_3$), 3.06 (s, 3H, N-C$\underline{H}_3$), 3.32 (br. t, 2H, N-C$\underline{H}_2$), 4.33 (q, *J* = 6.9 Hz, 1H, C$\underline{H}$-CH_3) 4.45-4.60 (m, 4H, -N-C$\underline{H}_2$-C$\underline{H}_2$-O), 7.15 (d, *J* = 8.3 Hz, 1H, ArH^3), 7.66 (dd, *J* = 8.4 Hz, *J* = 7.3 Hz, 1H, ArH^6), 8.42 (dd, *J* = 8.5 Hz, *J* = 1.1 Hz, 1H, ArH^2), 8.47 (d, *J* = 8.2 Hz, 1H, ArH^7), 8.57 (dd, *J* = 7.3 Hz, *J* = 1.1 Hz, 1H, ArH^5).

Synthesis of 7–(3'–mercaptopropyloxy)-4–methylcoumarin (**6**)

Adapting a procedure from the literature,[56] K_2CO_3 (9.44 g, 68.31 mmol, 1.00 eq.) and KI (0.38 g, 2.29 mmol, 0.03 eq.) were added to the solution of 7–hydroxy-4–methylcoumarin (12.04 g, 68.34 mmol) and allylbromide (8.90 mL, 12.46 g, 102.99 mmol, 1.5 eq.) in DMF (100 mL). After stirring at 100 °C for 24 h under argon atmosphere, the mixture was cooled, and water (300 mL) was added. The precipitated raw product was filtered off, and crystallized repeatedly from ethanol (200 mL) to remove all impurities. Yield of 7-allyloxy-4-methylcoumarin **4**: 11.19 g (51.75 mmol, 76 %).

^{1}H-NMR (400 MHz in $CDCl_3$, δ in ppm): δ = 2.17 (d, *J* = 1.0 Hz, 3H, C*H*$_3$), 4.38 (dt, 2H, *J* = 1.4 Hz, *J* = 5.3 Hz, O-C*H*$_2$), 5.12 (dd, *J* = 1.2 Hz, *J* = 10.5 Hz, 1H, C*H*$_2^{cis}$=CH), 5.22 (dd, *J* = 1.4 Hz, *J* = 17.3 Hz, 1H, C*H*$_2^{trans}$=CH), 5.81 (m, 1H, CH_2=C*H*), 5.91 (br. q, *J* = 1.0 Hz, 1H, Coum*H*^{3}), 6.60 (d, *J* = 2.5 Hz, 1H, Ar*H*^{8}), 6.66 (dd, *J* = 2.5 Hz, *J* = 8.8 Hz, 1H, Ar*H*^{6}), 7.27 (d, *J* = 8.8 Hz, 1H, Ar*H*^{5}).

Subsequently, the mixture of intermediate 7–allyloxy-4–methylcoumarin **4** (2.00 g, 9.25 mmol), thioacetic acid (1.30 mL, 1.41 g, 18.50 mmol, 2.0 eq.) and AIBN (0.76 g 4.62 mmol, 0.5 eq.) in benzene (100 mL) was refluxed for 24 h. After cooling to room temperature, 10 wt% aqueous NaOH (70 mL) was added slowly and stirred for 10 min. The organic layer was separated and washed with more 10 wt% NaOH-solution (2 × 70 mL), water and brine (70 mL). The organic layer was dried over $MgSO_4$, and the solvent was evaporated. The residue was crystallized four times from ethanol, to yield 2.02 g (75 %) of 7–(3'–(acetylthio)propyloxy)-4–methylcoumarin **5**.

^{1}H-NMR (400 MHz in $CDCl_3$, δ in ppm): δ = 2.11 (tt, J = 6.6 Hz, 2H, S-CH_2-C*H*$_2$-CH_2-O), 2.35 (s, 3H, C*H*$_3$-COS), 2.40 (d, J = 1.1 Hz, 3H, Ar-C*H*$_3$), 3.07 (t, J = 7.1 Hz, 2H, S-C*H*$_2$), 4.07 (t, J = 6.1 Hz, 3H, O-C*H*$_2$), 6.14 (d, J = 1.1 Hz, 1H, Coum*H*^{3}), 6.80 (d, J = 2.5 Hz, 1H, 1H, Ar*H*^{8}), 6.85 (dd, J = 8.8 Hz, J = 2.5 Hz, 1H, Ar*H*^{6}), 7.49 (d, J = 8.8 Hz, 1H, Ar*H*^{5}).

The intermediate thioacetate **5** (0.63 g, 2.15 mmol) in ethanol (15 mL) is cooled to 0 °C. NaOH (0.50 g, 12.5 mmol, 5.8 eq.) was added, and the mixture was stirred overnight under argon atmosphere. Within the initial 1-2 h of the reaction, the mixture became clear. After acidifying the solution with conc. $HCl_{(aq)}$, a precipitate was formed, which was filtered off and washed with water. The raw product was dissolved in CH_2Cl_2 (40 mL), the organic phase washed with brine (20 and 50 mL), dried over $MgSO_4$, and the solvent removed under reduced pressure. The

intermediate 7-(3'-mercaptopropyloxy)-4-methylcoumarin **6** was obtained as slightly yellow solid. Yield: 0.52 g (2.08 mmol, 97 %).

^{1}H-NMR (400 MHz in $CDCl_3$, δ in ppm): δ = 1.40 (t, J = 8.1 Hz, 1H, S*H*), 2.12 (tt, J = 6.5 Hz, J = 6.4 Hz, 2H, S-CH_2-C*H*$_2$-CH_2-O), 2.40 (d, J = 1.1 Hz, 3H, -C*H*$_3$), 2.75 (dt, J = 7.0 Hz, J = 7.5 Hz, 2H, S-C*H*$_2$), 4.15, (t, J = 5.9 Hz, 2H, O-C*H*$_2$), 6.14 (d, J = 1.0 Hz, 1H, Coum*H*^{3}) 6.83 (d, J = 2.4 Hz, 1H, Ar*H*^{8}), 6.86 (dd, J = 8.8 Hz, J = 2.5 Hz, 1H, Ar*H*^{6}), 7.50 (d, J = 8.7 Hz, 1H, Ar*H*^{5}) (see Figure S3).

Synthesis of 4−(*N*'−dodecyl−*N*'−methyl)amino)-1,3dioxo−1H−benzo[de]isoquinolin-2(3H)−yl)ethyl 2−methyl-3−((((3−((4−methyl-2−oxo-2H−chromen-7−yl)oxy)propyl)thio)carbono-thioyl)thio)propanoate (**FRET-TTC**).

Triethylamine (0.32 mL, 0.23 g, 2.28 mmol, 1.1 eq.) was slowly added to 7−(3'−mercaptopropyloxy)-4−methylcoumarin **6** (0.39 g, 1.55 mmol) in CH_2Cl_2 (7 mL) while stirring. After 30 min, CS_2 (0.11 ml, 0.14 g, 1.82 mmol, 1.2 eq.) was added, and the solution was stirred for another 1 h. Then, a solution of naphthalimide derivative **3** (0.89 g, 1.55 mmol, 1.0 eq.) in CH_2Cl_2 (7 mL) was slowly added. The solution was stirred overnight at room temperature. The solvent was evaporated, and the residue purified by column chromatography (silicagel, gradient eluent petrolether/ethyl acetate 5:1 (v/v) increasing to 1:1 (v/v)). The product **FRET−TTC** was obtained as orange oil. Yield: 0.24 g (0.29 mmol, 19 %)

^{1}H-NMR (400 MHz in $CDCl_3$, δ in ppm): δ = 0.87 (t, *J* = 6.9 Hz, 3H, CH_2-C*H*$_3$), 1.24-1.29 (m, 18H, (C*H*$_2$)$_9$-CH_3), 1.57 (d, *J* = 7.4 Hz,1H, CH-C*H*$_3$) 1.73 (br. tt, 2H, N-CH_2-C*H*$_2$), 2.16 (tt, J^1= J^2= 6.5 Hz, 2H, S-CH_2-C*H*$_2$), 2.39 (d, *J* = 1.1 Hz, 3H, Coum-C*H*$_3$), 3.07 (s, 3H, N-C*H*$_3$), 3.33 (br. t, *J* = 7.4 Hz, 2H, N-C*H*$_2$), 3.46 (t, *J* = 7.1 Hz, 2H, S-C*H*$_2$), 4.05 (t, *J* = 6.0 Hz, 2H, Aryl-O-C*H*$_2$),

4.32-4.56 (m, 4H, N-(C$\underline{H}_2$)$_2$-OOC), 4.79 (q, J = 7.4 Hz, 1H, OOC-C$\underline{H}$-CH$_3$), 6.13 (d, J = 1.1 Hz, 1H, CoumH^3), 6.78 (d, J = 2.5 Hz, 1H, CoumH^6), 6.84 (dd, J = 8.8 Hz, J = 2.5 Hz, 1H, CoumH^8), 7.18 (d, J = 8.3 Hz, 1H, NaphH^3), 7.49 (d, J = 8.8 Hz, 1H, CoumH^5), 7.67 (dd, J = 7.9 Hz, J = 7.9 Hz, 1H, NaphH^6), 8.46-8.49 (m, 2H, NaphH^2 + NaphH^7), 8.57 (dd, J = 7.2 Hz, J = 1.0 Hz, 1H, NaphH^5). Attribution of signals confirmed by ^{1}H-^{1}H correlation (COSY) experiments.

^{13}C-NMR (75 MHz in $CDCl_3$, δ in ppm): δ = 14.22 ($\underline{C}$H$_3$-CH$_2$), 16.89 ($\underline{C}$H$_3$-CH-COO), 18.77 ($\underline{C}$H$_3$-Coum), 22.77 (CH$_3$-$\underline{C}$H$_2$), 27.11 (N-(CH$_2$)$_2$-$\underline{C}$H$_2$), 27.53 (N-CH$_2$-$\underline{C}$H$_2$-CH$_2$), 27.82 (S-CH$_2$-$\underline{C}$H$_2$), 29.43-29.71 (N-(CH$_2$)$_3$-($\underline{C}$H$_2$)$_6$), 32.00 (CH$_3$-CH$_2$-$\underline{C}$H$_2$), 33.34 (S-$\underline{C}$H$_2$-CH$_2$), 38.65 ((C=O)$_2$N-$\underline{C}$H$_2$), 41.77 (N-$\underline{C}$H$_3$), 48.26 (CH$_3$-$\underline{C}$H-COO), 57.34 (N-$\underline{C}$H$_2$-(CH$_2$)$_2$), 63.29 (COO-$\underline{C}$H$_2$), 66.73 (aryl-O-$\underline{C}$H$_2$), 101.64 (CoumC^8), 112.21 (CoumC^3), 112.57 (CoumC^6), 113.88 (CoumC^{4a}), 114.73 (NaphC^1 + C^3), 122.98 (NaphC^8), 125.16 (NaphC^6), 125.70 (CoumC^5), 126.02 (NaphC^{4a}), 130.51 (NaphC^{8a}), 131.29 (NaphC^7), 131.39 (NaphC^5), 132.82 (NaphC^2), 152.60 (CoumC^4), 155.35 (NaphC^{8a}), 161.36 (CoumC^7), 161.78 (CoumC^2=O), 164.10 ($\underline{C}$ON), 164.73 (NaphC^4), 170.97 ($\underline{C}$OO), 221.48 ($\underline{C}$=S). Attribution of signals confirmed by ^{1}H-^{13}C heteronuclear single quantum correlation (HSQC) and Heteronuclear Multiple Bond Correlation (HMBC) experiments.

Elemental analysis ($C_{44}H_{54}N_2O_7S_3$) calculated: C 64.52 %, H 6.65%, N 3.42 %, S 11.74% found: C 64.19 %, H 6.74 %, N 3.35 %, S 10.80 %

ESI: calculated mass M_r = 819.10 g/mol, found: 841.64 g/mol $[M+Na]^+$:

FTIR (selected bands cm^{-1}): 2924, 2852, 1730, 1693, 1653, 1612, 1585, 1514, 1466, 1452, 1387, 1369, 1354, 1292, 1281, 1263, 1240, 1201, 1147, 1068, 1024, 1016, 872, 849, 833, 816, 781, 760, 735, 706.

UV-vis absorbance: in CH_2Cl_2 (λ_{max}=424 nm, ε = 8500 $L \cdot mol^{-1} \cdot cm^{-1}$), in THF ($\lambda_{max}$=424 nm, ε = 10700 $L \cdot mol^{-1} \cdot cm^{-1}$)

Synthesis of polymers

In the typical procedure for homopolymers **pDMAm*** and **pNiPAm***, the monomer, initiator V-40 and chain transfer agent **FRET–TTC** were dissolved in benzene. The solution was purged with argon for 45 min and immersed into a preheated oil bath with a temperature of 90 °C. After stirring for a specific time, the reaction was stopped by opening the flask to the air and cooling the flask with liquid nitrogen. For chain extension block copolymerization, NIPAm and macro chain transfer agent **pDMAm*** were dissolved in benzene. A stock solution of V-40 in benzene (2 mg/mL) was prepared and an appropriate volume of this solution was added. The solution was purged with argon for 40 min and immersed into a preheated oil bath with a temperature of 90 °C. After stirring for a specific time, the reaction was stopped by opening the flask to the air and cooling the flask with dry ice/*i*-propanol. While homopolymer **pNiPAm*** was precipated successively in diethylether and in pentane, all other polymers were precipitated twice into diethylether for purification. The isolated polymers were dried in a vacuum oven, dissolved in distilled water and lyophilized. The detailed amounts engaged are specified in Table 1.

Table 1. Reaction conditions for polymerization in benzene (ca. 33 wt% monomer and RAFT chain transfer agent CTA) at 90 °C using initiator V-40

Sample	monomer M	amount of M [g]	CTA	amount of CTA [mg]	initiator I [mg]	molar ratio M:CTA:I	t [h]

pDMAm1*	DMAm	2.44	FRET–TTC	94	3.0	2050:10:1	10
pDMAm2*	DMAm	3.47	FRET–TTC	150	4.5	1940:10:1	3 [a)]
pNiPAm*	NiPAm	2.78	FRET–TTC	94	2.9	2050:10:1	15
pDMAm–*b*–pNiPAm1*	NiPAm	0.12	pDMAm1*	500	0.57	450:10:1	20
pDMAm–*b*–pNiPAm2*	NiPAm	0.47	pDMAm2*	1500	2.2	450:10:1	3 [a)]

[a)] 50 ca. wt% solids monomer and CTA

Methods and instrumentation

Elemental analysis was done with a Vario ELIII microanalyzer (Elentar Analysensysteme, Hanau, Germany). NMR spectra were recorded with a spectrometer Avance 300 (Bruker) operating at 300 MHz (^{1}H), and 75 MHz (^{13}C) respectively. Chemical shifts δ are reported in ppm vs. the respective solvent peaks at δ (1H) 4.79 ppm for D_2O, and δ (^{1}H) 7.26 ppm and δ (^{13}C) 77.16 ppm for $CDCl_3$. Fourier-transform infrared (FTIR) spectra were taken in the ATR mode with a spectrometer Nicolet Avatar 370 FT-IR (Thermo Fisher Scientific) equipped with an AMTIR crystal and an ATR Smart Performer element.

UV/Vis spectra were recorded on a Lambda 25 UV/Vis Spectrometer (Perkin Elmer) in quartz sample cells (path length 1 cm). Assuming one naphthalimide chromophore in each macromolecule due to the 'R'-group of the **FRET-TTC**, number average molar masses M_n^{UV} were calculated by end group analysis via UV vis spectroscopy from the absorbance at λ_{max} = 424 nm in CH_2Cl_2. Values were calculated according to $M_n^{UV} = \varepsilon \cdot c \cdot d \cdot E^{-1}$ where ε [$L \cdot mol^{-1} \cdot cm^{-1}$] is the extinction coefficient, c [$g \cdot L^{-1}$] is the concentration of the polymer in solution and d [cm] is the

optical path length. The molar extinction coefficient ε of the naphthalimide chromophore in the polymers was taken as 8500 $L \cdot mol^{-1} \cdot cm^{-1}$ at 424 nm, assuming to be identical to the value determined for **FRET-TTC** in CH_2Cl_2.

Temperature-dependent static fluorescence experiments were performed with a thermostated fluorimeter FluoroLog-3 (HORIBA Jobin Yvon, France). Optical silica cuvettes with an optical path length d = 1 cm were used. The excitation wavelength was set to 318 nm, and emission wavelength to 376 nm for the coumarin chromophore and to 520 nm for the naphthalimide chromophore. Temperature was precise within 1 K. The polymer samples were dissolved in Millipore water or in the tetradecyldimethylamine–*N*–oxide TDMAO/decane microemulsion.

Size exclusion chromatography (SEC) was performed by a self-made apparatus with simultaneous UV and RI detection at room temperature (flow rate 0.5 mL·min-1). The stationary phase was a 300 x 8 mm_2 PSS GRAM linear M column (7 µm particle size), with eluent 0.1% LiBr in NMP (injection volume 100 µL). Samples were filtered through 0.45 µm filters. The system was calibrated with narrowly distributed polystyrene standards (PSS, Mainz, Germany).

Thermogravimetric analysis (TGA) was performed under N_2 atmosphere using an apparatus SDTA851e (Mettler-Toledo, Gießen/Germany, heating rate of 10 K min^{-1}). Differential scanning calorimetry (DSC) employed an apparatus DSC822e (Mettler-Toledo, Gießen/ Germany), applying heating and cooling rates of 10 K min^{-1} for the first and second, and 30 K min^{-1} for the third and fourth heating and cooling cycles. Glass transition temperatures T_g were taken from the second heating cycle that used a heating rate of 10 K min^{-1} via the midpoint method.[78]

The temperature dependent transmittance was recorded with a Cary 5000 (Varian) spectrometer at 600 nm with heating and cooling rates of 0.5 $K \cdot min^{-1}$. Temperatures are precise within 0.5 K. The

temperature at which the solution's transmittance starts to decrease ('onset') was taken as cloud point (CP). Dynamic light scattering (DLS) was performed with a high performance particle Sizer (HPPS-5001, Malvern Instrument, Malvern/UK) equipped with a He-Ne laser beam and a thermoelectric Peltier element to control the temperature. The backscattering mode was used at a scattering angle of Θ = 173 °. Samples were diluted with ultrapure water to the desired concentration, and measured in heating runs by raising the temperature in steps of 1 °C equilibrating the sample for 120 s prior to each measurement.

More comprehensive static (SLS) and dynamic (DLS) light scattering experiments were performed with a 3DSpectrometer (LSinstruments, Switzerland). The instrument is equipped with a He-Ne laser and operates at a wavelength $\lambda = 632.8\,\mathrm{nm}$. All measurements were carried out with an angle scan (2θ) between 30 and 135° in 5° steps and a temperature ramp from 20 to 60 °C in 5 °C steps. At each angle three repetitions were performed with a duration of 60 s.

The static intensity was deduced according to $I^{\mathrm{SLS}}_{\mathrm{sample}}(q) = \frac{C_{\mathrm{n,sample}} - C_{\mathrm{n,solvent}}}{C_{\mathrm{n,toluene}}} \cdot R_{\mathrm{toluene}}$, where $q = \frac{4\pi n_0}{\lambda} \sin\frac{2\theta}{2}$ is the magnitude of the scattering vector, $C_{\mathrm{n},i} = \frac{C_i}{P_i}$ is the count rate C divided by the laser power P of species i, and $R_{\mathrm{toluene}} = 1.37 \cdot 10^{-5}\ \mathrm{cm}^{-1}$ is the Rayleigh ratio of toluene for the given laser wavelength.[79] For calculating the apparent molecular weight of aggregates, $I(0)$ is needed and was estimated via a Guinier fit, using eq. 1, in the q-range of 0.0066–0.0128 nm^{-1} (30–60°).

$$I(q) = I(0) \cdot \exp\left(-R_{\mathrm{g}}^2 q^2/3\right) \quad (1)$$

The effective aggregation number ($N^{\mathrm{eff}}_{\mathrm{agg}}$) from the obtained $I(0)$ values, was estimated according to: $N^{\mathrm{eff}}_{\mathrm{agg}} = \frac{I(0)}{K \cdot c_g \cdot M}$ (2)

with $K = \frac{4\pi^2 n_0^2}{N_A \lambda^4}\left(\frac{dn}{dc_g}\right)^2$, where K is the optical constant which corresponds to the value reported for polyDMAm,[80] c_g the mass concentration of polymer in solution, M the molar mass (M_n^{theo} is used for calculation), n_0 the refractive index of the solvent, $\frac{dn}{dc_g}$ the refractive index increment for the polymer in solution, and N_A the Avogadro constant. The refractive index increment values were determined experimentally with an Orange Analytics 19" dn/dc instrument. The DLS data were analyzed based on the optimized regularization techniques (ORT). [81, 82] The analysis was performed with SimplightQt (Python based software for analyzing light scattering data). Starting with the measured intensity autocorrelation function ($g^{(2)}(\tau) - 1$), the field autocorrelation function ($g^{(1)}(\tau)$) was calculated via the Siegert relation: $g^{(2)}(\tau) - 1 = \beta \cdot \left(g^{(1)}(\tau)\right)^2$ where β is the coherence factor and an instrument specific parameter below 1. The size distributions were analyzed by using a set of log-normal distributions instead of bell-shaped B-splines as reported in [17,18]. From the analysis a weight is obtained for each contribution.

$$g^{(1)}(\tau) = \sum_i w_i g_i^{(1)}(\tau) \quad (3)$$

where $g^{(1)}(\tau)$ is the field autocorrelation function, w_i the weight and $g_i^{(1)}(\tau)$ the Laplace transform of the underlying correlation time distribution of the i^{th} component.

$$g_i^{(1)}(\tau) = \int_0^\infty L(\tau, \tau_i, \sigma_i) \cdot \exp\left(-\frac{\tau}{\tau_i}\right) d\tau \quad (4)$$

The correlation time distribution $L(\tau, \tau_i, \sigma_i)$ is defined as

$$L(\tau, \tau_i, \sigma_i) = \frac{1}{\sqrt{2\pi}\sigma_i \tau} \exp\left(-\frac{(\ln(\tau) - \ln(\tau_i))^2}{2 \cdot \sigma_i^2}\right) \quad (5)$$

where τ_i is the median and σ_i the standard deviation of the distribution. The apparent hydrodynamic radius is obtained via the Stokes-Einstein-Smoluchowski equation ($R_h^{app} = k_B T/(6\pi\eta D)$, where k_B is the Boltzmann constant, T the absolute temperature and η the solvent

viscosity) from the diffusion coefficient ($D_i = \frac{q^2}{\tau_i}$, where q is the magnitude of the scattering vector).

RESULTS AND DISCUSSION

The two-fold fluorescently labelled RAFT chain transfer agent **FRET-TTC** bears the coumarin donor chromophore as part of the deactivating so-called 'Z-group' (forming the ω-end group of polymers synthesized with the RAFT agent), and the naphthalimide acceptor dye as part of the re-initiating 'R-group' (forming the α-end group of polymers synthesized with the RAFT agent). **FRET-TTC** was synthesized via seven steps starting from 7–hydroxy-4−methylcoumarin ('4–methylumbelliferone') and 4–chloro−1,8–naphthalic anhydride. Despite its complexity, the ^{1}H NMR spectrum of **FRET-TTC** displays a number of well-resolved aromatic proton signals (Figure 2), which can be unambiguously attributed to either the coumarin (*e.g.*, signals 35, 40 and 43) or the naphthalimide chromophores (*e.g.*, signals 16, 22 and 24). A priori, this enables not only the end group analysis of the molar masses of polymers which are devoid of aromatic protons, synthesized with this RAFT agent by ^{1}H NMR spectroscopy using either end group, as it is typical for most (meth)acrylic polymers including pDMAm and pNiPAm. Also, their direct comparison, *i.e.*, the molar ratio of incorporated R and Z groups, allows for estimating the preservation of trithiocarbonate moiety ('end group fidelity'), and thus of the 'livingness' of the RAFT polymerization process.[39, 83, 84] Additionally, the intense UV-vis absorbance at about 425 nm of the naphthalimide chromophore attached to the R-group enables end group analysis of the molar masses of polymers of virtually any chemical structure by an additional, independent method.[84]

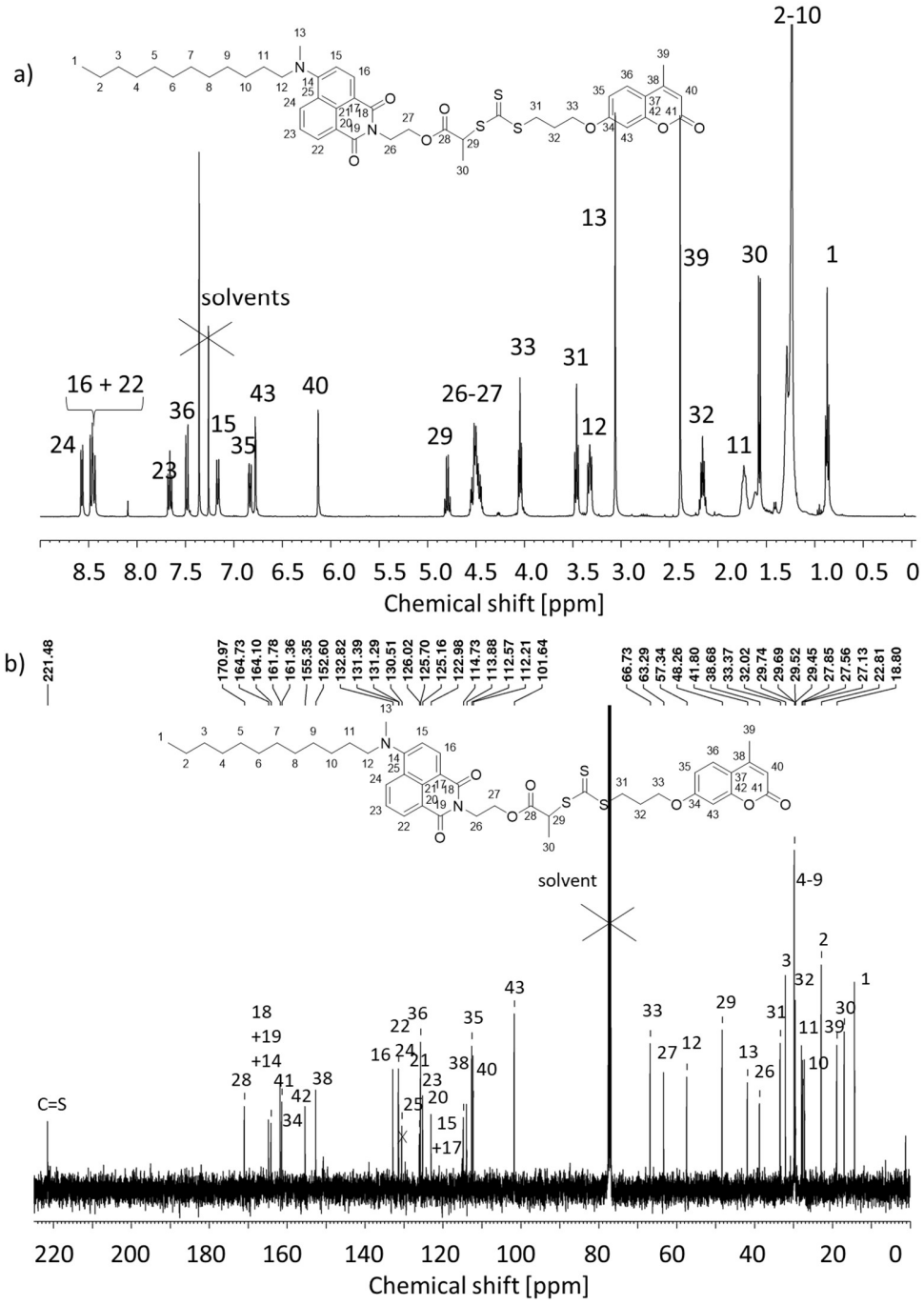

a)

Figure 2. NMR spectra of two-fold fluorescently labelled **FRET-TTC** in $CDCl_3$: (a) ^{1}H-NMR, (b) ^{13}C-NMR.

As illustrated in Figure 3, the emission maximum of the coumarin chromophore is at about 376 nm, while the emission maximum of the naphthalimide chromophore is at about 520 nm. Importantly, the emission maximum of the coumarin matches very well the absorbance band of the naphthalimide between 350 and 480 nm. Furthermore, the coumarin has its excitation maximum at about 324 nm, which coincides with the excitation minimum of the naphthalimide chromophore in the UV-region (318 nm). Thus, the combined coumarin (as donor) and naphthalimide (as acceptor) chromophores incorporated into the functional RAFT agent **FRET–TTC** represent a well-suited pair of fluorophores for FRET.

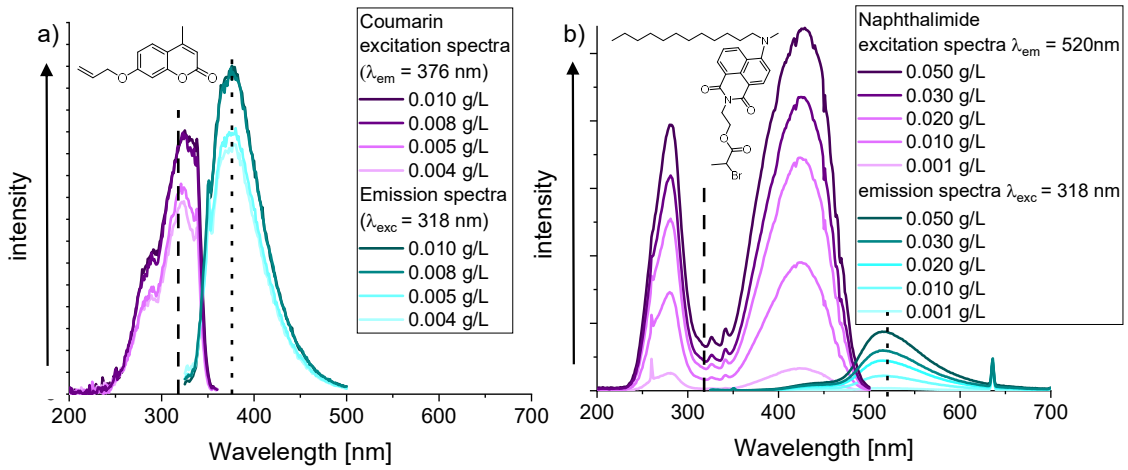

Figure 3. Fluorescence spectra in tetrahydrofuran for intermediates (a) 7-allyloxy-4-methylcoumarin **4** (emission spectra excited at 318 nm, excitation spectra recorded by emission at 376 nm), and (b) naphthalimide **3** (emission spectra excited at 318 nm, excitation spectra recorded by emission at 520 nm). Excitation spectra are shown in magenta (emission wavelength indicated as dashed vertical line), and emission spectra in blue color (excitation wavelength indicated as broken vertical line), the shades intensifying with increasing dye concentration.

Chain transfer agent **FRET−TTC** was successfully employed in the RAFT polymerization of acrylamides, for obtaining homopolymers **pDMAm*** and **pNiPAm***, and block copolymer **pDMAm−b−pNiPAm*** adapting an established procedure (*cf.* Table 1).[39] The reactions proceeded rather slowly, requiring 10 – 20 h and high monomer concentrations to achieve conversions in the range of 60 – 90 %, which might be due to the bulkiness of the bi-functionalized trithiocarbonate. Still, when the concentration of monomer and chain transfer agent was increased from 33 to 50 wt%, the duration of the reaction could be reduced to 3 h. Table 2 summarizes the results of the polymerization. The molar masses determined by different methods match reasonably well with each other within the precision of the methods, and also with the theoretically expected ones. Further, the dispersities Đ are rather low. Importantly, the molar mass distributions of all polymers were monomodal, and the molar masses of the **pDMAm*** samples increased after chain extension polymerization with NiPAm (see Figure S4). This indicates the successful synthesis of block copolymers **pDMAm−b−pNIPAm1*** and **pDMAm−b−pNiPAm2***.

Table 2. Molecular characterization of the polymers synthesized (*cf.* Figure 1). The applied reaction conditions and chain transfer agents are specified in Table 1.

Polymer	Yield [%] [a]	Monomer conversion [%] [b]	M_n^{theo} [kg mol^{-1}] [c]	DP_n^{theo} [d]	M_n^{NMR} [kg mol^{-1}] [e]	DP_n^{NMR} [f]	Z/R [g]	M_n^{UV} [kg mol^{-1}] [h]	M_n^{app} [kg mol^{-1}] [i]	Đ [j]
pDMAm1*	61	80	17	166	34	334	0.9	22	16	1.25

pDMAm2*	80	81	16	157	22	217	1.0	15	20	1.21
pNIPAm*	69	88	25	180	36	311	-	20	27	1.23
pDMAm-b-pNiPAm1*	48 [k)]	58	25	26	39	34	0.8	23	24	1.43
pDMAm-b-pNiPAm2*	84 [l)]	81	21	37	30	64	-	20	28	1.26

[a)] by gravimetry; [b)] by ^{1}H-NMR analysis of the raw reaction mixture; [c)] theoretically expected number average molar mass, calculated as the molar ratio of the monomer to the RAFT agent employed [M]/[CTA] corrected by the monomer conversion as determined by ^{1}H-NMR, assuming ideal ('living') conditions for the RAFT process;[12, 39] [d)] theoretically expected number average degree of polymerization of the newly added polymer block; [e)] number average molar mass determined by end group analysis via ^{1}H-NMR, using the integrals of the aromatic protons of the naphthalimide moiety (from R-group), [f)] number average degree of polymerization of the newly added polymer block via ^{1}H-NMR analysis, [g)] relative α,ω-end group fidelity, by comparing the integrals of the ^{1}H-NMR of the aromatic protons of the naphthalimide (from R group) and coumarin (from Z-group) moieties, [h)] number average molar mass determined by end group analysis via UV/Vis spectroscopy in dichloromethane using the band at λ_{max} = 424 nm (ε = 8500 L·mol^{-1}·cm^{-1}), [i)] apparent number average molar mass determined by SEC (calibration with polystyrene standards), full elution diagams shown in Figure S4, [j)] dispersity Đ = M_w/M_n from SEC analysis, [k)] pDMAm1* used as macroCTA, [l)] pDMAm2* used as macroCTA. Precision of all molar mass values is ± 20 %.

Moreover, the signals of the end groups were clearly visible in the ^{1}H NMR spectra and could be resolved for the naphthalimide and coumarin moieties despite the relatively high molar masses (Figure 4 and Figure S5). The accordingly derived Z/R ratios are close to unity. Only when the NiPAm content of the polymers becomes high, the signal of the NH-group interferes too strongly

with the end group signals (Figure 4b) to allow for a meaningful determination of the Z/R ratio. All these findings point to a well-controlled polymerization process. Note that compared to the ^{1}H NMR spectra of the polymers in $CDCl_3$, the characteristic signals of the end groups, in particular of the R-group, were markedly broadened and attenuated when the spectra are recorded in D_2O. This points to a poor solvation of the end groups and possibly their aggregation into hydrophobic nanodomains.

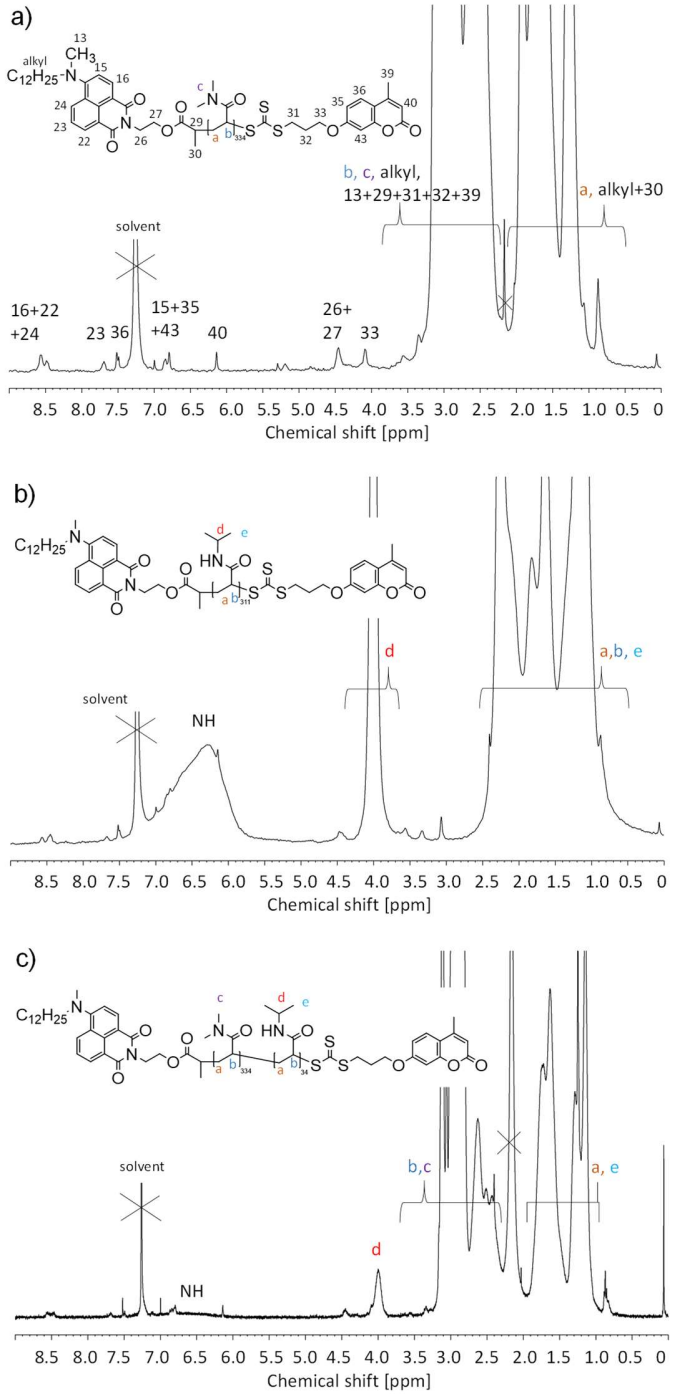

Figure 4. ^{1}H NMR spectra of two-fold fluorescently labelled polymers in $CDCl_3$: (a) **pDMAm1***, (b) **pNiPAm*** , (c) **pDMAm–b–pNiPAm1***.

According to thermogravimetric analysis TGA, all polymers were thermally stable up to at least 200°C. Significant mass losses were observed only when the temperature exceeded 300 °C. Differential scanning calorimetry DSC revealed a glass transition for homopolymers **pDMAm1*** at 118 °C and **pNiPAm*** at 132 °C, in good agreement with the literature.[39, 85] Block copolymer **pDMAm–b–pNiPAm1*** showed only one glass transition at 122 °C, *i.e.*, a value between those of the respective homopolymers. This is an indication that the two polyacrylamide blocks are compatible in the bulk phase and do not (micro)phase separate.

Behavior in aqueous media

All the polymers synthesized were directly soluble in water at ambient temperature. However, in contrast to the behavior of the solutions of homopolymers **pDMAm1*** and **pDMAm2***, the solutions of block copolymers **pDMAm−b−pNiPAm1*** and **pDMAm−b−pNiPAm2*** became turbid upon heating beyond 35 °C (Figure 5). The solution of reference homopolymer **pNiPAm*** showed a cloud point CP of 26 °C. Accordingly, the attachment of the two fluorophores at chain ends reduced the phase transition temperature of about 31−32 °C which is typically reported for atactic pNiPAm samples of comparable molar mass,[18, 21, 22, 86] by a few degrees. As the α-end group with the dodecyl chain and the large naphthalimide fluorophore, i.e. the hydrophobic sticker group B, is too hydrophobic to affect the CP of pNiPAm,[83, 87-91] its lowering for **pNiPAm*** is presumably due to the ω-end group with the coumarin fluorophore. The moderately reduced CP in comparison with other end-group effects reported, suggests that the effective hydrophobicity of the ω-end group is lower than the one of end groups bearing a naphthyl, azobenzene or dodecyl moiety.[92-94]

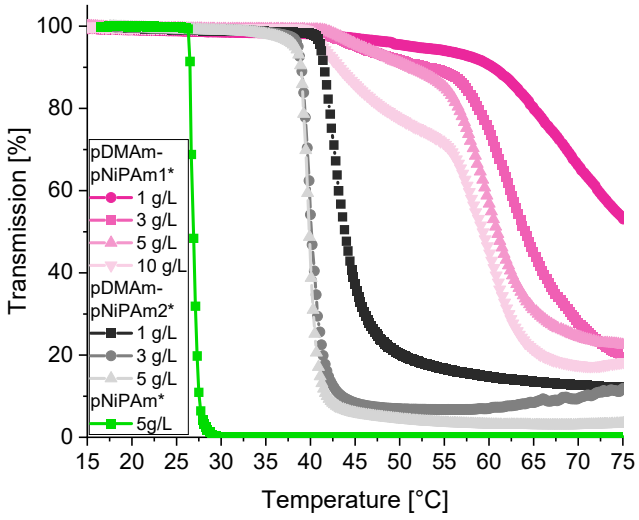

Figure 5. Optical transmittance measurements for aqueous solutions of homopolymer **pNiPAm*** (left curve, green), and block copolymers **pDMAm–b–pNiPAm1*** (right curves, magenta), and **pDMAm–b–pNiPAm2*** (center curves, grey), for varying concentrations (heating runs). The onset of decline in transmittance is taken as cloud point.

CP values of the block copolymers **pDMAm−b−pNiPAm1*** and **pDMAm−b−pNiPAm2*** were 40 °C and 36 °C, respectively, which are substantially higher than for homopolymer reference **pNiPAm***. The increase is attributed to the covalent attachment of the pNiPAm block to a large hydrophilic polymer. The numerous reports of this general effect in the literature include also the specific case of block copolymers made from DMAm and NiPAm.[66-68, 94, 95] The effect is the more pronounced the shorter the pNiPAm block is, as observed for samples **pDMAm−b−pNiPAm1*** and **pDMAm−b−pNiPAm2***. Also, the CP's shift with increasing concentration slightly to lower

temperatures for both polymers, again in agreement with the literature for such dilute solutions.[20] After the heating run, the polymers separated macroscopically in a polymer rich and polymer poor phase, so that no cooling cycle was applied. However, under stirring, the polymer dispersions were stable, and the clouding transitions were found fully reversible. A closer inspection of the evolution of turbidity with increasing temperature reveals a striking difference between the two block copolymers. Whereas the clouding transition is sharp and pronounced for **pDMAm−b−pNiPAm2***, indicating the rapid formation of rather large aggregates once the phase transition temperature is crossed, the turbidity of the solutions of **pDMAm−b−pNiPAm1*** evolves in two stages. In a first step, the drop of transmittance is small, before in a second step the solutions become opaque at about 15 °C higher than CP. Qualitatively, this suggests the formation of small aggregates initially, which transform into much larger ones only after further dehydration of the polymer coils at more elevated temperatures.

An analogous behavior was observed in dynamic light scattering (DLS) experiments (Figure 6). While the solutions of homopolymers **pDMAm1*** and **pDMAm2*** showed virtually temperature independent scattering behavior, the solution of **pNiPAm*** exhibited a sudden and steep increase of the polymers Z-average hydrodynamic diameter D_H upon heating to 27°C. Also the solutions of block copolymers **pDMAm−b−pNiPAm1*** and **pDMAm−b−pNiPAm2*** showed a marked increase of the D_H upon heating at 41 °C and 38 °C, respectively.

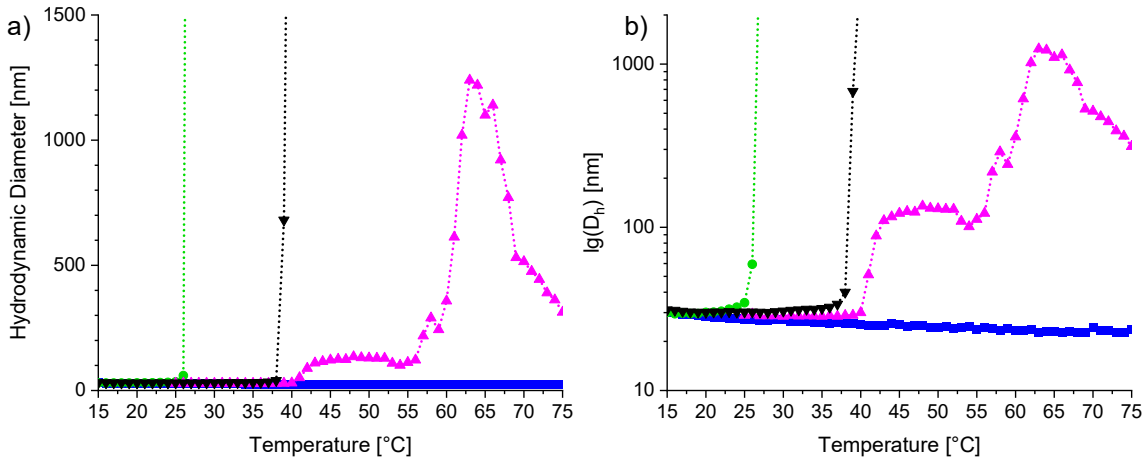

Figure 6. Temperature dependent evolution of the Z-average hydrodynamic radius D_h of polymers **pDMAm1*** (■), **pNiPAm*** (●), **pDMAm–b–pNiPAm1*** (▲), and **pDMAm–b–pNiPAm2*** (▼) in aqueous solution (5 g·L^{-1}), followed by DLS (HPPS-5001, Malvern Instrument, Malvern/UK) in (a) linear and (b) semi-logarimthmic presentation. Dashed lines are meant as guide to the eye..

Moreover, Figure 6 reveals that independently whether they are permanently hydrophilic or thermo-responsive, all of the two-fold fluorescently labelled polymers display D_h values of about 25 nm. This suggests the formation of small aggregates due to the surfactant-like structure of the α-terminal hydrophobic end group.[40, 96, 97] When heating beyond the cloud point, homopolymer **pNiPAm*** as well as block copolymer **pDMAm–b–pNiPAm2*** immediately form large aggregates (with D_h >1 µm). In contrast, block copolymer **pDMAm–b–pNiPAm1*** shows an apparent two-step transition above the cloud point. Initially, aggregate size increases slowly to a moderate value (D_h ≈ 125 nm), but rises markedly only above 55 °C. The two-step aggregation matches the observations on the clouding transitions (Figure 5) discussed above. We attribute the differing aggregation behavior of the two block copolymers to the considerably shorter thermo-

responsive pNiPAm block in copolymer **pDMAm–b–pNiPAm1***. Notwithstanding the possible differences between the specific aggregation processes, the DLS experiments demonstrate the temperature-controlled transition of associating BAA* to BAB* systems for the block copolymers studied, as sketched in Scheme 1.

Fluorescence Spectroscopy of Aqueous Polymer Solutions and Microemulsions

The temperature-dependent fluorescence of the two-fold labelled polymers in aqueous media was studied with the fixed excitation wavelength of 318 nm (Figure 7). At this wavelength, the excitation of the donor fluorophore is efficient but of the acceptor fluorophore at a minimum (*cf.* Figure 3), and thus, the spectra are sensitive to the FRET process. Figure 7 reveals on a first view that the spectra of all polymer–solvent systems are subject to changes with increasing temperature. Furthermore, these changes vary markedly not only between the different polymers studied, but also when pure water as solvent (Figure 7a, c, e) is replaced by a TDMAO–decane microemulsion (Figure 7b, d, f).

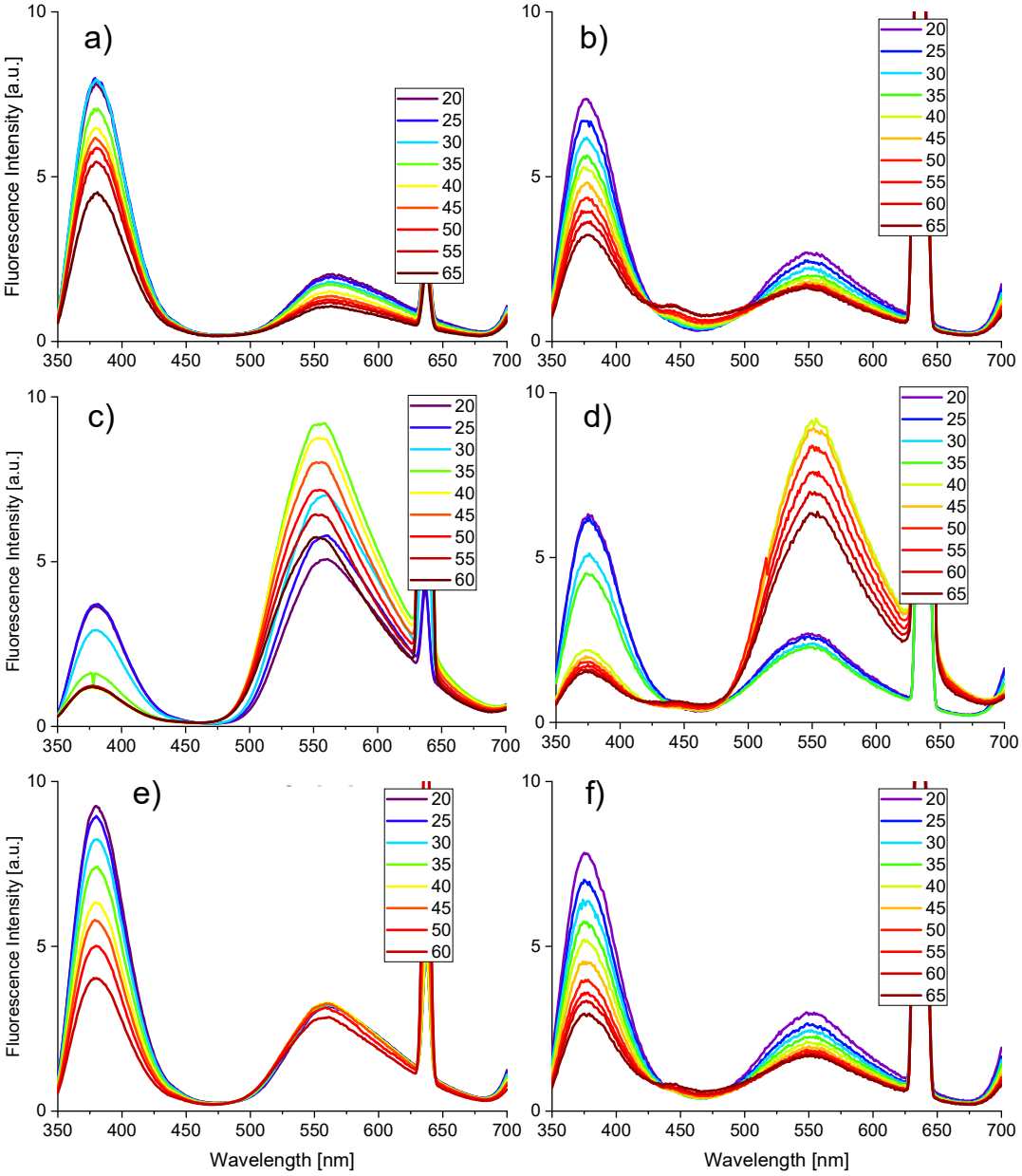

Figure 7: Temperature-dependent fluorescence of solutions (1 g·L^{-1}) of **pDMAm1*** (a-b), **pNiPAm*** (c-d) and **pDMAm–b–pNiPAm1*** (e-f) in pure water (a, c, e) and microemulsion (b, d, f; 190 mM TDMAO in decane).

The spectra were analyzed with respect to the position of the emission maximum of the acceptor fluorophore, *i.e.*, possible solvatochromism of the naphthalimide, and to the relative emission intensities of the donor and acceptor chromophores, *i.e.*, possible changes in the extent of FRET occurring (Figure 8). In pure aqueous solution, we note that the emission maximum of the acceptor chromophore is located at 561 nm below 25 °C for all polymers studied. This value corresponds to a surrounding of the chromophore close to pure water.[73] Whereas the peak position did not change between 15 and 65 °C for permanently hydrophilic homopolymer **pDMAm1***, a hypsochromic shift of about 10 nm was observed for thermoresponsive homopolymer **pNiPAm*** in this temperature range with increasing temperature (Figure 8a). The value indicates a less, though still highly polar surrounding of the chromophore at elevated temperatures, which could, for instance, be equivalent to a mixture of water and N-methylformamide.[73] It is also evident that the solvatochromic shift does not occur linearly, but seems to follow an S-shape with the maximum slope between 25 and 35 °C, *i.e.*, around the cloud point of **pNiPAm***. The combined findings suggest that the shift is a consequence of the coil-to-globule collapse of the pNiPAm chains and their concomitant partial desolvation, changing the local environment of the fluorophore from 'nearly aqueous' to 'water-swollen NiPAm groups'. In the case of block copolymer **pDMAm–b–NiPAm1***, a similar behavior is seemingly observed, though being much less pronounced. The hypsochromic shift amounts only to about 2 nm, and the maximum slope of the S-shaped curve seems shifted to higher temperatures, between 30 and 45 °C (Figure 8a). Again, this behavior can be correlated with the cloud point transition of the block copolymer. The weakness of the solvatochromic shift compared to the homopolymer may be easily explained by the much shorter pNiPAm block in the copolymer, as well as by the separation of the collapsed pNiPAm block and the naphthalimide moiety by the long pDMAm block in between.[75]

It is interesting to note that the form of the fluorescence spectra of **pDMAm–b–NiPAm1*** did not alter upon dilution down to a concentration of 1 mg L^{-1} (lowest concentration studied). Neither the positions of the emission maxima nor the intensity ratio between the donor and acceptor bands changed. This suggests that the hairy micelles exist still at such low concentrations, and that any critical aggregation concentration must be lower than 10^{-7} M, if existing at all.

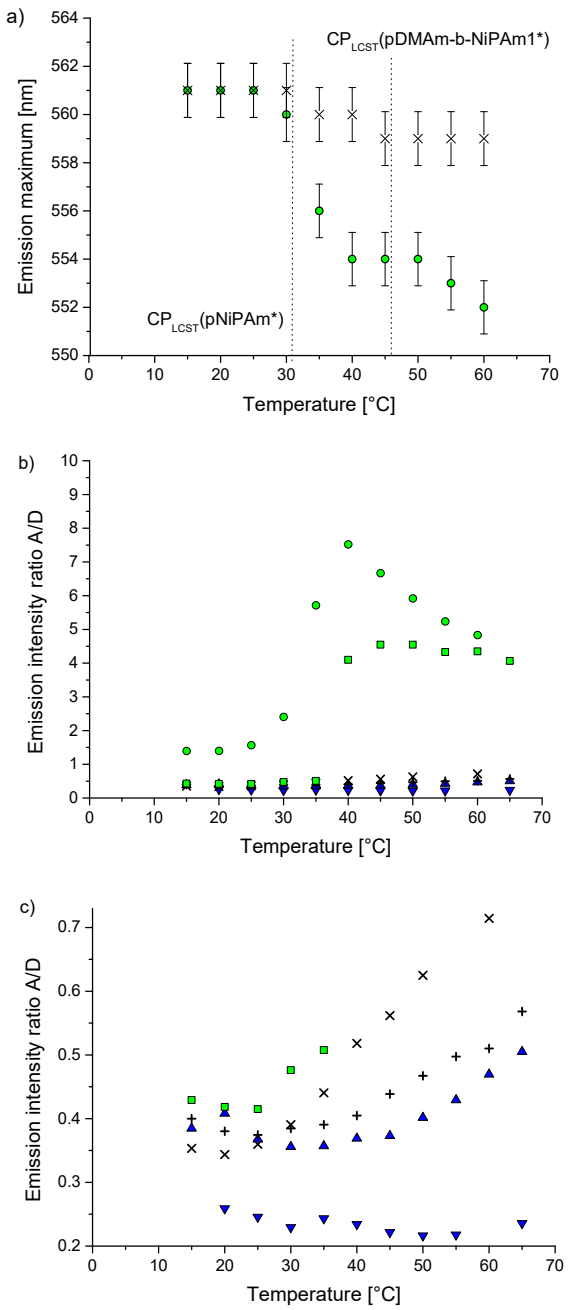

Figure 8: Temperature-dependent fluorescence of solutions (1 g·L^{-1}) of **pDMAm1*** (▼, ▲), **pNiPAm*** (●, ■,), and **pDMAm–b–pNiPAm1*** (×, +) in pure water (▼, ●, ×) and in 190 mM TDMAO in decane (▲, ■, +): (a) shift of the acceptor emission maximum with temperature; (b) intensity ratio of acceptor emission / donor emission ; (c) magnified section of (b).

When analyzing the temperature-dependent relative emission intensities of the donor and acceptor chromophores, *i.e.*, the extent of FRET of the polymers in pure water (Figure 8b-c), the structure-dependent effects seem to follow an analogous pattern as discussed for the solvatochromism. While the extent of FRET is virtually independent of the temperature for the homopolymer reference **pDMAm1***, a strong increase of FRET is seen for the reference **pNiPAm*** just above its cloud point. The extent of FRET increases also for block copolymer **pDMAm–b–pNiPAm1*** when crossing the cloud point (Figure 8c), but the effect is much weaker than for **pNiPAm*** (Figure 8b).

The picture differs characteristically when the polymers are dissolved in the TMDAO–decane microemulsion. The position of the emission maximum of the acceptor fluorophore is located at 551 nm for **pDMAm1*** and **pDMAm–b–NiPAm1*** at all temperatures, and also for **pNiPAm*** at temperatures above 30 °C. This indicates a less, though still highly polar surrounding of the chromophore in the presence of the microemulsion's oil droplets compared to the pure aqueous solution. Interestingly, below 30°C, the emission maximum of **pNiPAm*** is further hypsochromically shifted to 548 nm, indicating an even less polar surrounding at low temperatures. Concerning the temperature-dependent extent of FRET, the general behavior is rather similar to the one observed in pure aqueous solution (Figure 8b). The FRET efficiency is strongly enhanced for **pNiPAm*** when crossing the cloud point, whereas temperature effects are small for the permanently hydrophilic reference **pDMAm1*** and the block copolymer. Figure 8c shows that overall, at room temperature, the extent of FRET is slightly higher for **pDMAm1*** and **pDMAm–b–NiPAm1*** in the microemulsion compared to the aqueous solution. Still, a closer look reveals important differences between **pDMAm1*** and **pDMAm–b–NiPAm1*** in the

microemulsion when heated. On the one hand, the FRET effect increases continuously, albeit very slightly, for **pDMAm1*** with increasing temperature, in contrast to its virtual independence in pure water. On the other hand, the increase of FRET for **pDMAm–b–NiPAm1*** when passing the cloud point is markedly weaker in micromemulsion than in water, and parallels the behavior of **pDMAm1*** (Figure 8c).

Combining the findings of the fluorescence studies, the following picture emerges. (i) In water at ambient temperature, the acceptor dye is not located in the hydrophobic domain of micellar aggregates, but rather at their interface. The moderately hydrophobic ω–termini with the donor dye are neither located in the hydrophobic domain of micellar aggregates nor do they tend to approach the micelles surface, either by backfolding of the polymer chains or by bridging different micelles. (ii) The solvatochromic effects suggest that the hydrophobic sticker group B has a marked affinity for inserting into the oil droplets of the microemulsion; (iii) The distance between α– and ω–termini of the permanently hydrophilic polymer is virtually unaffected by temperature. (iv) The coil-to-globule collapse transition of α–ω-two-fold fluorophore labeled polymers separated by a thermo-sensitive polymer chain, here pNiPAm, increases FRET strongly. Still, it cannot be distinguished whether the effect indicates an increased backfolding of the ω–termini with loop formation to form flower micelles, or whether it is mainly due to the inherent contraction of the chain conformation above CP and the concomitant reduction of the average end-to-end distance of the chains, thus approaching the donor and acceptor chromophores. (v) The block copolymer shows little backfolding, if at all. It forms hairy micelle in the BAA* state (cf. Scheme 1b left). In the BAB* state, the extent of backfolding of the B* block might be slightly higher than in the A* state, but if so, the increase is very limited. The same reasoning applies to the possibility of bridging micellar cores. Importantly, backfolding is further reduced in the microemulsion

compared to in the pure aqueous solution. This implies that the collapsed pNiPAm segments of the copolymer have little tendency to assemble onto oil droplet interface, let alone to enter the oil droplets. Accordingly, the scenario sketched on the lower right side of Scheme 1b seems predominant. This means, that the polymer micelles are interconnected by clusters of collapsed pNiPAm chains, eventually forming a network with two different, alternating types of crosslinks formed by micellar cores (or oil droplets, respectively) and by pNiPAm microdomains.

Static (SLS) and Dynamic Light Scattering (DLS) Results for Aqueous Polymer Solutions and Microemulsions

More detailed light scattering experiments of the pure polymers in aqueous solution as a function of temperature in the range from 20 to 60 °C showed distinctly different behavior for the three types of polymer studied. As expected, the homopolymer reference **pDMAm1*** shows very little effect of temperature (just some shift to shorter relaxation times with increasing temperature that can largely be attributed to the reduced water viscosity) and very similar correlation functions (Figure 9a), dominated by a rather monoexponential decay and some tailing for longer times. This shows that small micellar aggregates are present with a hydrodynamic radius R_h of 10-15 nm (Figure 9b). This is in good agreement with the simple picture of having aggregated dodecyl chains surrounded by the permanently hydrophilic pDMAm shell. The unchanged state of aggregation is confirmed by the static light scattering (SLS) intensity measured for concentrations of 1.0 to 10.0 g L^{-1} from 20 to 60 °C (Figure 9c). No change of aggregation is seen in this temperature range, and aggregation numbers of 20 to 80 are observed, which generally decrease with increasing

concentration. The tailing seen in DLS might be attributed to overlapping polymer chains, as often seen for polymers.

In the case of the thermo-responsive reference homopolymer **pNiPAm***, the situation is clearly different. A fast decay of the correlation function is still present, but slower than for **pDMAm1***. For lower temperature, a second, even slower decay is noted (Figure 9d). This can be interpreted such that the 10-15 nm R_h sized micelles are still seen, but with a pNiPAm shell instead of a pDMAm shell. They are partly aggregated, presumably in dynamic equilibrium, into clusters of about 800 nm in radius (Figure 9e; note that the results were obtained with a different instrument than those in Fig.6, focussing on correctly measuring longer correlation times. For the data displayed in Figure 6, measurements simply run out of the experimental size observation window of the instrument). This must be due to attractive forces arising from the presence of the pNiPAm block.[97] With increasing temperature, pNiPAm is expected to shrink in size and lead to stronger attractive interactions. This is manifested by the decreasing value of R_h which reaches a value of 40–50 nm for 55 °C (Figure 9e). SLS (Figure 9f) shows that single micelles are present still at 20 °C. However upon reaching 25 °C, the pNiPAm shall provides sufficiently attractive interactions to induce clustering. Figure 9f also demonstrates that the clusters retain their size as a function of temperature. Only for the highest concentration of 10 g L^{-1}, some growth occurs above 45 °C. This suggests that the shrinkage seen by DLS corresponds to a compaction of the formerly more loosely connected micellar aggregates.

Strikingly, the diblock copolymer **pDMAm–b–NiPAm1*** shows a behavior somewhere in between of the two homopolymers. In DLS (Figure 9g), monomodal decay is observed, which becomes much slower for temperatures above 40 °C. At lower temperatures, we see in Figure 9h, as for the homopolymer references, small individual micellar aggregates with $R_{h\ values}$ of 10–15 nm.

These agglomerate at higher temperature into clusters with R_h values of 150–250 nm, increasing in size with rising temperature. Apparently, the pDMAm block reduces the attractive interaction exerted by the pNiPAm block, and clustering occurs only above the phase transition temperature of the thermo-responsive block. This is mirrored by the SLS results (Figure 9i) which show a constant aggregation number of about 20 until 35 °C, irrespective of the concentration. Above 35 °C, the aggregation increase number substantially, approaching a constant value for temperatures above 45 °C. The total aggregation number of ~2000 macromolecules corresponds to a situation where about 100 of the copolymer micelles are contained within bigger clusters of R_h = 150-250 nm. This means that these are rather weakly compacted aggregates.

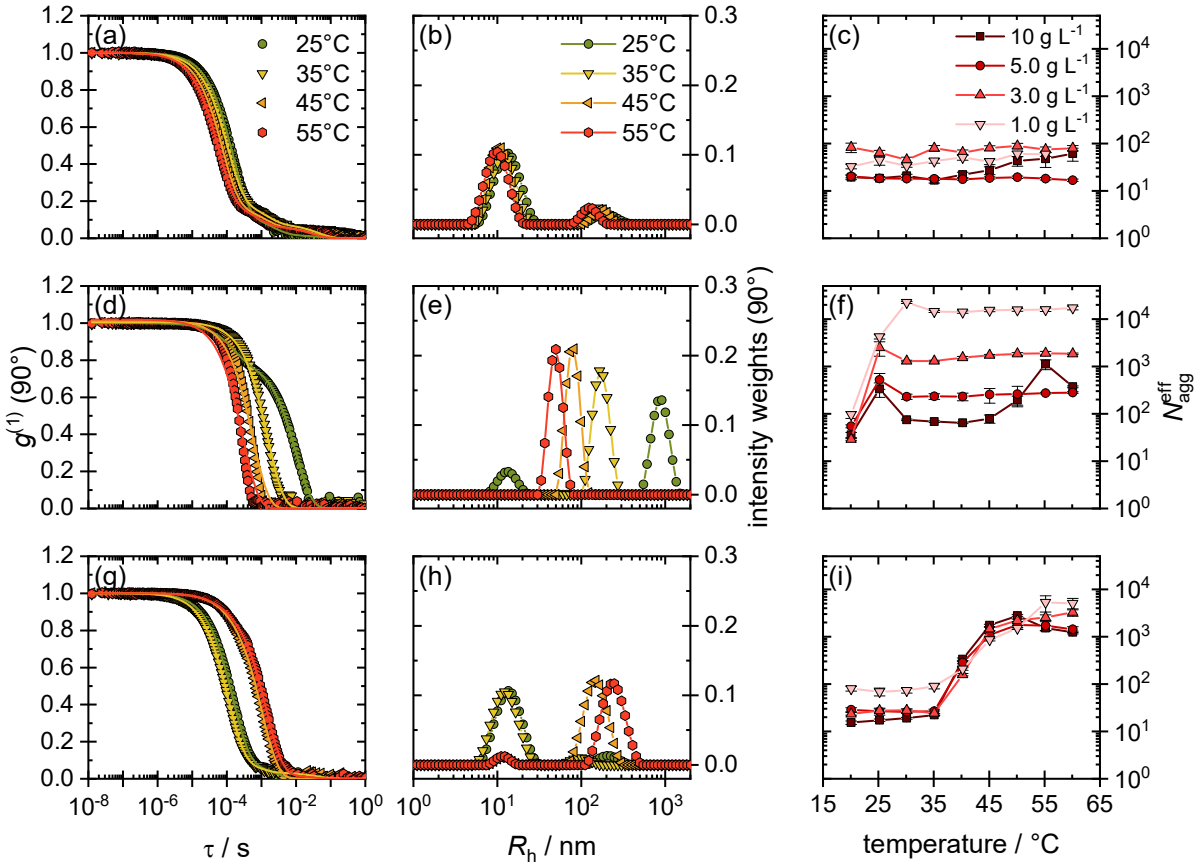

Figure 9. Field correlation curves obtained from DLS measurements (LSinstruments) (a): **pDMAm1***, (d): **pNiPAm***, (g): **pDMAm–b–NiPAm1***) and corresponding intensity weighted

size distribution of the pure polymer solutions ((b): **pDMAm1***, (e): **pNiPAm***, (h): **pDMAm–b–NiPAm1***), obtained from the measurement at 90° and a concentration of 3.0 g L^{-1}. The corresponding fit curves of the correlation functions are shown as solid lines. In addition, we show the effective aggregation number calculated based on the estimated forward scattering intensity $I(0)$ obtained via a Guinier fit, by using eq. 2, as a function of temperature ((c): **pDMAm1***, (f): **pNiPAm***, (i): **pDMAm–b–NiPAm1***).

For the microemulsion based systems, the DLS measurements showed basically a negligible effect of the presence of the different polymers, except for the case of **pNiPAm*** (Table 3, the corresponding autocorrelation functions are shown in Figure S6). This can be interpreted such that the lifetime of binding of an individual micromulsion droplet in the clusters is shorter than the relevant measurement time, which is in the range of ~1 ms. Accordingly, their diffusion occurs rather freely. Only for the polymers with a pNiPAM shell, the hydrophobic binding becomes apparently strong enough at high temperature so that the clustering of the microemulsion droplets becomes so extensive, that their diffusion is substantially slowed down and clusters of a mean radius of ~ 100 nm are generated.

Table 3. Collective diffusion coefficient D and hydrodynamic radius R_h for the pure TDMAO/decane o/w microemulsion (ME) and its mixtures with the different polymers. Data are obtained from the corresponding simple exponential fit of the initial slope of the autocorrelation function. R_h was calculated by the Stokes-Einstein relation. Errors of the last digit are given in parentheses.

Sample	ME		ME + **pDMAm1***		ME + **pNiPAm***		ME + **pDMAm-b-NiPAm1***	
	25°C	55°C	25°C	55°C	25°C	55°C	25°C	55°C
D / μm^2 s^{-1}	76.8(4)	113(2)	65.2(6)	144(2)	64.4(6)	4.59(5)	66.2(5)	149.2(9)
R_h / nm	3.20(9)	4.24(13)	3.76(11)	3.31(9)	3.81(12)	103(4)	3.71(11)	3.20(9)

In summary, it can be stated that the tendency for clustering of these micellar aggregates depends on temperature and can be largely controlled via the type of block attached. For the purely hydrophilic pDMAm sample, no clusters are observed. In contrast, clustering takes place for the pNiPAm sample already above 20 °C, *i.e.* below the cloud point, with a marked tendency for shrinkage with increasing temperature. The diblock **pDMAm–b–NiPAm*** system requires temperatures above 35 °C, *i.e.*, to reach the coil-to-globule transition of the thermo-responsive block, to undergo clustering of its micelles, and the cluster size increases somewhat with increasing temperature.

CONCLUSIONS

Nonionic water-soluble polyacrylamides labelled with complementary fluorophores at the opposite termini of the chains were synthesized, which are suited for intramolecular FRET. The precise placement of the fluorophores is conveniently achieved by using a bi-functional trithiocarbonate (**FRET-TTC**) as chain transfer agent in RAFT polymerizations. Employing a coumarin of the methylumbelliferone family as donor and a 4-aminonaphthalimide as acceptor groups, the polymers show effective FRET with a large spectral shift between excitation (at 318 nm) and emission (at 560 nm) wavelengths. Moreover, the marked hydrophobic character

supported by an *n*-dodecyl substituent renders the acceptor chromophore effective as hydrophobic end group ('sticker') for designing polymeric surfactants. Two-fold labelled macroRAFT agents **pDMAm***, which were first synthesized from *N,N*-dimethylacrylamide (DMAm) using **FRET-TTC**, could be successfully chain extended by *N*-isopropylacrylamide (NiPAm). The pNiPAm block of the produced dual hydrophilic block copolymers is thermo-responsive, showing an LCST transition in aqueous media. Due to the hydrophobic sticker group containing the acceptor fluorophore, these block copolymers **pDMAm-b-pNiPAm*** represent 'smart' polymeric surfactants. At low temperature, they behave as B-A-A* systems forming hairy micelles. At elevated temperatures, above the LCST-type phase transition of pNiPAm switching its character from water-soluble to insoluble, they behave as associative telechelics BAB* with unsymmetrical hydrophobic end blocks (A, A*= hydrophilic block, B, B* = hydrophobic block). This allows for switching the surfactant properties significantly by a thermal stimulus, inducing *e.g.* the formation of large aggregates as required for associative thickeners. Interestingly, the findings from fluorescence experiments suggest that the aggregation at elevated temperatures is not due to the conventional bridging of flower-micelles by the BAB*-type polymers. In fact, FRET gives no evidence for increased backfolding or bridging by the polymer chains above the coil-to-collapse transition of the pNiPAm block. Instead of, it appears that hairy micelles persist, which are connected to larger assemblies by separate microdomains of collapsed pNiPAm blocks at the end of the 'hairs'. This picture is confirmed by light scattering experiments, which show that the presence of the pNiPAm block alone is sufficient to induce cluster formation of the micelles present above 20 °C, where the clusters shrink substantially with increasing temperature. In contrast, the BAB*-type polymer shows the more typical pNiPAm transition around 35 °C, also leading to clusters of micelles. However in this case, the clusters increase somewhat in size with

increasing temperature. In general, the aggregation behavior of these polymers can be tuned largely by temperature, and such a behavior can be expected to boost the thickening and gelling efficiency of such block copolymers compared to conventional BAB associative thickeners. Accordingly, such unsymmetrically end-capped thermo-responsive water-soluble polymers represent a promising design for both 'smart' and particularly efficient rheology modifiers. The tendency for the particular structure formation of these polymers is enhanced when exchanging pure water as solvent by an o/w microemulsion.

ASSOCIATED CONTENT

Supporting Information.

The supporting information is available free of charge at https://pubs.acs.org./doi/10.1021/acs.langmuir.xyz

SEC elugrams of the polymers studied, solution ^{1}H NMR spectra of diblock copolymer **pDMAm-pNiPAm2*** and key intermediates in the synthesis of chain transfer agent **FRET-CTA**, and field correlation functions of the polymers in the microemulsion in dependence on the correlation time τ together with decay rates as function of scattering vector q at 25 and 55 °C (PDF)

AUTHOR INFORMATION

Corresponding Authors

* Prof. Michael Gradzielski, E-mail: michael.gradzielski@tu-berlin.de, Address: Technische Universität Berlin, Stranski-Laboratorium für Physikalische und Theoretische Chemie TC7, FG

Physical Chemistry/ Molecular Material Science Institute of Chemistry, Strasse des 17. Juni 124, 10623 Berlin, Germany

* Prof. André Laschewsky, E-mail: laschews@uni-potsdam.de, Address: Universität Potsdam, Institut für Chemie, Karl-Liebknecht-Strasse 24-25, 14476 Potsdam-Golm, Germany

AUTHOR CONTRIBUTIONS

The manuscript was written through contributions of all authors. All authors have given approval to the final version of the manuscript.

FUNDING SOURCES

This work was supported by Deutsche Forschungsgemeinschaft (DFG), grants GR 1030/22-1 and LA 611/17-1.

ACKNOWLEDGMENT

The authors gratefully acknowledge support for fluorescence spectroscopy by K. Brennenstuhl and M. Kumke (Universität Potsdam) as well as by A. Gessner and in particular O. Sakhno (Fraunhofer IAP). They also acknowledge the support for SEC analysis by S. Prenzel and H. Schlaad, and for thermal analysis by D. Schanzenbach (all Universität Potsdam).

CONFLICT OF INTEREST

The authors declare no conflict of interest.

REFERENCES

1. Förster, S.; Antonietti, M., Amphiphilic Block Copolymers in Structure-Controlled Nanomaterial Hybrids. *Adv. Mater.* **1998,** *10*, 195-217.
2. Halperin, A., Polymeric vs. Monomeric Amphiphiles: Design Parameters. *J. Macromol. Sci. C: Polym. Rev.* **2006,** *46*, 173-214.
3. Börner, H. G.; Schlaad, H., Bioinspired functional block copolymers. *Soft Matter* **2007,** *3*, 394-408.
4. Mai, Y.; Eisenberg, A., Self-assembly of block copolymers. *Chem. Soc. Rev.* **2012,** *41*, 5969-5985.
5. Zhulina, E. B.; Borisov, O. V., Theory of Block Polymer Micelles: Recent Advances and Current Challenges. *Macromolecules* **2012,** *45*, 4429-4440.
6. Hebbeker, P.; Steinschulte, A. A.; Schneider, S.; Plamper, F. A., Balancing Segregation and Complexation in Amphiphilic Copolymers by Architecture and Confinement. *Langmuir* **2017,** *33*, 4091-4106.
7. Raffa, P.; Wever, D. A. Z.; Picchioni, F.; Broekhuis, A. A., Polymeric Surfactants: Synthesis, Properties, and Links to Applications. *Chem. Rev.* **2015,** *115*, 8504-8563.
8. Laschewsky, A., Molecular Concepts, Self-organisation and Properties of Polysoaps. *Adv. Polym. Sci.* **1995,** *124*, 1-86.
9. Li, L.; Raghupathi, K.; Song, C.; Prasad, P.; Thayumanavan, S., Self-assembly of random copolymers. *Chem. Commun.* **2014,** *50*, 13417-13432.
10. Liu, S.; Armes, S. P., Recent advances in the synthesis of polymeric surfactants. *Curr. Opin. Coll. Interface Sci.* **2001,** *6*, 249-256.
11. Barner, L.; Davis, T. P.; Stenzel, M. H.; Barner-Kowollik, C., Complex Macromolecular Architectures by Reversible Addition Fragmentation Chain Transfer Chemistry: Theory and Practice. *Macromol. Rapid Commun.* **2007,** *28*, 539-559.
12. Moad, G.; Rizzardo, E.; Thang, S. H., Living Radical Polymerization by the RAFT Process – A Third Update. *Aust. J. Chem.* **2012,** *65*, 985-1076.
13. Laschewsky, A.; Herfurth, C.; Miasnikova, A.; Stahlhut, F.; Weiss, J.; Wieland, C.; Wischerhoff, E.; Gradzielski, M.; Malo de Molina, P., Stars and Blocks: Tailoring Polymeric Rheology Modifiers for Aqueous Media by Controlled Free Radical Polymerization. *ACS Symp. Ser.* **2013,** *1148*, 125-143.
14. Hruby, M.; Štěpánek, P.; Pánek, J.; Papadakis, C. M., Crosstalk between responsivities to various stimuli in multiresponsive polymers: change in polymer chain and external environment polarity as the key factor. *Colloid Polym. Sci.* **2019,** *297*, 1383-1401.
15. Cohen Stuart, M. A.; Huck, W. T. S.; Genzer, J.; Müller, M.; Ober, C.; Stamm, M.; Sukhorukov, G. B.; Szleifer, I.; Tsukruk, V. V.; Urban, M.; Winnik, F.; Zauscher, S.; Luzinov, I.; Minko, S., Emerging applications of stimuli-responsive polymer materials. *Nat. Mater.* **2010,** *9*, 101-113.
16. Moad, G., RAFT polymerization to form stimuli-responsive polymers. *Polym. Chem.* **2017,** *8*, 177-219.
17. Mukherji, D.; Marques, C. M.; Kremer, K., Smart Responsive Polymers: Fundamentals and Design Principles. *Annu. Rev. Condens.Matter Phys.* **2020,** *11*, 271-299.
18. Schild, H. G., Poly(N-isopropylacrylamide): Experiment, theory and application. *Prog. Polym. Sci.* **1992,** *17*, 163-249.
19. Aseyev, V.; Tenhu, H.; Winnik, F., Temperature dependence of the colloidal stability of neutral amphiphilic polymers in water. *Adv. Polym. Sci.* **2006,** *196*, 1-85.

20. Aseyev, V.; Tenhu, H.; Winnik, F., Non-ionic Thermoresponsive Polymers in Water. *Adv. Polym. Sci.* **2011,** *242*, 29-89.
21. Halperin, A.; Kröger, M.; Winnik, F. M., Poly(N-isopropylacrylamide) Phase Diagrams: Fifty Years of Research. *Angew. Chem. Int. Ed.* **2015,** *54*, 15342-15367.
22. Futscher, M. H.; Philipp, M.; Müller-Buschbaum, P.; Schulte, A., The Role of Backbone Hydration of Poly(N-isopropyl acrylamide) Across the Volume Phase Transition Compared to its Monomer. *Sci. Rep.* **2017,** *7*, [17012] 1-10.
23. Karg, M.; Pich, A.; Hellweg, T.; Hoare, T.; Lyon, L. A.; Crassous, J. J.; Suzuki, D.; Gumerov, R. A.; Schneider, S.; Potemkin, I. I.; Richtering, W., Nanogels and Microgels: From Model Colloids to Applications, Recent Developments, and Future Trends. *Langmuir* **2019,** *35*, 6231-6255.
24. Luo, G.-F.; Chen, W.-H.; Zhang, X.-Z., 100th Anniversary of Macromolecular Science Viewpoint: Poly(N-isopropylacrylamide)-Based Thermally Responsive Micelles. *ACS Macro Lett.* **2020,** *9*, 872-881.
25. Afroze, F.; Nies, E.; Berghmans, H., Phase transitions in the system poly(N-isopropylacrylamide)/water and swelling behaviour of the corresponding networks. *J. Mol. Struct.* **2000,** *554*, 55-68.
26. Dimitrov, I.; Trzebicka, B.; Müller, A. H. E.; Dworak, A.; Tsvetanov, C. B., Thermosensitive water-soluble copolymers with doubly responsive reversibly interacting entities. *Prog. Polym. Sci.* **2007,** *32*, 1275-1343.
27. Strandman, S.; Zhu, X. X., Thermo-responsive block copolymers with multiple phase transition temperatures in aqueous solutions. *Prog. Polym. Sci.* **2015,** *42*, 154-176.
28. Laschewsky, A.; Müller-Buschbaum, P.; Papadakis, C. M., Thermo-responsive Amphiphilic Di- and Triblock Copolymers Based on Poly(N-isopropyl¬acrylamide) and Poly(methoxy diethylene glycol acrylate): Aggregation and Hydrogel Formation in Bulk Solution and in Thin Films. *Prog. Colloid Polym. Sci.* **2013,** *140*, 15-34.
29. Skrabania, K.; Kristen, J.; Laschewsky, A.; Akdemir, Ö.; Hoth, A.; Lutz, J.-F., Design, Synthesis, and Aqueous Aggregation Behavior of Nonionic Single and Multiple Thermoresponsive Polymers. *Langmuir* **2007,** *23*, 84-93.
30. Wyman, I. W.; Liu, G., Micellar structures of linear triblock terpolymers: Three blocks but many possibilities. *Polymer* **2013,** *54*, 1950-1978.
31. Bütün, V.; Liu, S.; Weaver, J. V. M.; Bories-Azeau, X.; Cai, Y.; Armes, S. P., A brief review of 'schizophrenic' block copolymers. *React. Funct. Polym.* **2006,** *66*, 157-165.
32. Papadakis, C. M.; Müller-Buschbaum, P.; Laschewsky, A., Switch It Inside-Out: "Schizophrenic" Behavior of All Thermoresponsive UCST–LCST Diblock Copolymers. *Langmuir* **2019,** *35*, 9660-9676.
33. Zehm, D.; Laschewsky, A.; Liang, H.; Rabe, J. P., Straightforward Access to Amphiphilic Dual Bottle Brushes by Combining RAFT, ATRP, and NMP Polymerization in One Sequence. *Macromolecules* **2011,** *44*, 9635-9641.
34. Zhao, B., Shape-Changing Bottlebrush Polymers. *J. Phys. Chem. B* **2021,** *125*, 6373-6389.
35. Chassenieux, C.; Nicolai, T.; Benyahia, L., Rheology of associative polymer solutions. *Curr. Opin. Coll. Interface Sci.* **2011,** *16*, 18-26.
36. Quienne, B.; Pinaud, J.; Robin, J.-J.; Caillol, S., From Architectures to Cutting-Edge Properties, the Blooming World of Hydrophobically Modified Ethoxylated Urethanes (HEURs). *Macromolecules* **2020,** *53*, 6754-6766.

37. Cook, M. T.; Haddow, P.; Kirton, S. B.; McAuley, W. J., Polymers Exhibiting Lower Critical Solution Temperatures as a Route to Thermoreversible Gelators for Healthcare. *Adv. Funct. Mater.* **2021,** *31*, [2008123] 1-25.
38. Herfurth, C.; Laschewsky, A.; Noirez, L.; von Lospichl, B.; Gradzielski, M., Thermoresponsive (star) block copolymers from one-pot sequential RAFT polymerizations and their self-assembly in aqueous solution. *Polymer* **2016,** *107*, 422-433.
39. Hechenbichler, M.; Laschewsky, A.; Gradzielski, M., Poly(N,N-bis(2-methoxyethyl)acrylamide), a thermoresponsive non-ionic polymer combining the amide and the ethyleneglycolether motifs. *Colloid Polym. Sci.* **2021,** *299*, 205-219.
40. Vagias, A.; Papagiannopoulos, A.; Kreuzer, L. P.; Giaouzi, D.; Busch, S.; Pispas, S.; Müller-Buschbaum, P., Effects of Polymer Block Length Asymmetry and Temperature on the Nanoscale Morphology of Thermoresponsive Double Hydrophilic Block Copolymers in Aqueous Solutions. *Macromolecules* **2021,** *54*, 7298-7313.
41. Dormidontova, E. E., Micellization Kinetics in Block Copolymer Solutions: Scaling Model. *Macromolecules* **1999,** *32*, 7630-7644.
42. Hayward, R. C.; Pochan, D. J., Tailored Assemblies of Block Copolymers in Solution: It Is All about the Process. *Macromolecules* **2010,** *43*, 3577-3584.
43. Gradzielski, M.; Duvail, M.; de Molina, P. M.; Simon, M.; Talmon, Y.; Zemb, T., Using Microemulsions: Formulation Based on Knowledge of Their Mesostructure. *Chem. Rev.* **2021,** *121*, 5671-5740.
44. Taribagil, R. R.; Hillmyer, M. A.; Lodge, T. P., Hydrogels from ABA and ABC Triblock Polymers. *Macromolecules* **2010,** *43*, 5396-5404.
45. Lakowicz, J. R., *Principles of Fluorescence Spectroscopy*. 3rd ed.; Springer: Boston, MA, 2006; p 954.
46. Farinha, J. P. S.; Martinho, J. M. G., Resonance Energy Transfer in Polymer Nanodomains. *J. Phys. Chem. C* **2008,** *112*, 10591-10601.
47. Rajdev, P.; Ghosh, S., Fluorescence Resonance Energy Transfer (FRET): A Powerful Tool for Probing Amphiphilic Polymer Aggregates and Supramolecular Polymers. *J. Phys. Chem. C* **2018,** *123*, 327-342.
48. Li, C.; Hu, J.; Liu, S., Engineering FRET processes within synthetic polymers, polymeric assemblies and nanoparticles via modulating spatial distribution of fluorescent donors and acceptors. *Soft Matter* **2012,** *8*, 7096-7102.
49. Ringsdorf, H.; Simon, J.; Winnik, F. M., Hydrophobically-modified poly(N-isopropylacrylamides) in water: probing of the microdomain composition by nonradiative energy transfer. *Macromolecules* **1992,** *25*, 5353-5361.
50. Ringsdorf, H.; Simon, J.; Winnik, F. M., Hydrophobically modified poly(N-isopropylacrylamides) in water: a look by fluorescence techniques at the heat-induced phase transition. *Macromolecules* **1992,** *25*, 7306-7312.
51. Ringsdorf, H.; Sackmann, E.; Simon, J.; Winnik, F. M., Interactions of liposomes and hydrophobically-modified poly-(N-isopropylacrylamides): an attempt to model the cytoskeleton. *Biochim. Biophys. Acta* **1993,** *1153*, 335-344.
52. Martin, T. J.; Webber, S. E., Fluorescence Studies of Polymer Micelles: Intracoil Direct Energy Transfer. *Macromolecules* **1995,** *28*, (26), 8845.
53. Wang, Y.; Kausch, C. M.; Chun, M.; Quirk, R. P.; Mattice, W. L., Exchange of Chains between Micelles of Labeled Polystyrene-*block*-poly(oxyethylene) As Monitored by Nonradiative Singlet Energy Transfer. *Macromolecules* **1995,** *28*, 904-911.

54. Rager, T.; Meyer, W. H.; Wegner, G.; Winnik, M. A., Influence of Chain Length and Salt Concentration on Block Copolymer Micellization. *Macromolecules* **1997,** *30*, 4911-4919.
55. Mizusaki, M.; Morishima, Y.; Winnik, F. M., Hydrophobically Modified Poly(sodium 2-acrylamido-2-methylpropanesulfonate)s Bearing Octadecyl Groups: A Fluorescence Study of Their Solution Properties in Water. *Macromolecules* **1999,** *32*, 4317-4326.
56. Oh, J. K.; Stöeva, V.; Rademacher, J.; Farwaha, R.; Winnik, M. A., Synthesis, Characterization, and Emulsion Polymerization of Polymerizable Coumarin Derivatives. *J. Polym. Sci., Part A: Polym. Chem.* **2004,** *42*, 3479-3489.
57. Wu, Y.; Hu, H.; Hu, J.; Liu, T.; Zhang, G.; Liu, S., Thermo- and Light-Regulated Formation and Disintegration of Double Hydrophilic Block Copolymer Assemblies with Tunable Fluorescence Emissions. *Langmuir* **2013,** *29*, 3711-3720.
58. Li, D.; Jiang, J.; Huang, Q.; Wang, G.; Zhang, M.; Du, J., Light-triggered "on-off" switching of fluorescence based on a naphthopyran-containing compound polymer micelle. *Polym. Chem.* **2016,** *7*, 3444-3450.
59. Matejiček, P.; Uhlík, F.; Limpouchová, Z.; Procházka, K.; Tuzar, Z.; Webber, S. E., Experimental Study of Hydrophobically Modified Amphiphilic Block Copolymer Micelles Using Light Scattering and Nonradiative Excitation Energy Transfer. *Macromolecules* **2002,** *35*, 9487-9496.
60. Matějíček, P.; Humpolíčková, J.; Procházka, K.; Tuzar, Z.; Špírková, M.; Hof, M.; Webber, S. E., Hybrid Block Copolymer Micelles with Partly Hydrophobically Modified Polyelectrolyte Shells in Polar and Aqueous Media: Experimental Study Using Fluorescence Correlation Spectroscopy, Time-Resolved Fluorescence, Light Scattering, and Atomic Force Microscopy. *J. Phys. Chem. B* **2003,** *107*, 8232-8240.
61. Chen, M.; Ghiggino, K. P.; Mau, A. W. H.; Rizzardo, E.; Sasse, W. H. F.; Thang, S. H.; Wilson, G. J., Synthesis of Functionalized RAFT Agents for Light Harvesting Macromolecules. *Macromolecules* **2004,** *37*, 5479-5481.
62. Li, C.; Zhang, Y.; Hu, J.; Cheng, J.; Liu, S., Reversible Three-State Switching of Multicolor Fluorescence Emission by Multiple Stimuli Modulated FRET Processes within Thermoresponsive Polymeric Micelles. *Angew. Chem. Int. Ed.* **2010,** *49*, 5120-5124.
63. Roth, P. J.; Haase, M.; Basché, T.; Theato, P.; Zentel, R., Synthesis of heterotelechelic α-ω dye functionalized polymer by the RAFT process and energy transfer between the end groups. *Macromolecules* **2010,** *43*, 895-902.
64. Huang, P.; Song, H.; Zhang, Y.; Liu, J.; Cheng, Z.; Liang, X.-J.; Wang, W.; Kong, D.; Liu, J., FRET-enabled monitoring of the thermosensitive nanoscale assembly of polymeric micelles into macroscale hydrogel and sequential cognate micelles release. *Biomater.* **2017,** *145*, 81-91.
65. Reeve, J. R.; Thomas, R. K.; Penfold, J., Surface Activity of Ethoxylate Surfactants with Different Hydrophobic Architectures: The Effect of Layer Substructure on Surface Tension and Adsorption. *Langmuir* **2021,** *37*, 9269-9280.
66. Convertine, A. J.; Lokitz, B. S.; Vasileva, Y.; Myrick, L. J.; Scales, C. W.; Lowe, A. B.; McCormick, C. L., Direct Synthesis of Thermally Responsive DMA/NIPAM Diblock and DMA/NIPAM/DMA Triblock Copolymers via Aqueous, Room Temperature RAFT Polymerization. *Macromolecules* **2006,** *39*, 1724-1730.
67. Zhou, Y.; Jiang, K.; Song, Q.; Liu, S., Thermo-Induced Formation of Unimolecular and Multimolecular Micelles from Novel Double Hydrophilic Multiblock Copolymers of N,N-Dimethylacrylamide and N-Isopropylacrylamide. *Langmuir* **2007,** *23*, 13076-13084.

68. Skrabania, K.; Li, W.; Laschewsky, A., Synthesis of Double-Hydrophilic BAB Triblock Copolymers via RAFT Polymerisation and their Thermoresponsive Self-Assembly in Water. *Macromol. Chem. Phys.* **2008,** *209*, 1389-1403.
69. Ida, S.; Morimura, M.; Kitanaka, H.; Hirokawa, Y.; Kanaoka, S., Swelling and mechanical properties of thermoresponsive/hydrophilic conetworks with crosslinked domain structures prepared from various triblock precursors. *Polym. Chem.* **2019,** *10*, 6122-6130.
70. Zehm, D.; Lieske, A.; Stoll, A., On the Thermoresponsivity and Scalability of N,N-Dimethylacrylamide Modified NIPAM Microgels. *Macromol. Chem. Phys.* **2020,** *221*, [2000018] 1-16.
71. Keddie, D. J.; Moad, G.; Rizzardo, E.; Thang, S. H., RAFT Agent Design and Synthesis. *Macromolecules* **2012,** *45*, 5321-5342.
72. Felorzabihi, N.; Froimowicz, P.; Haley, J. C.; Bardajee, G. R.; Li, B.; Bovero, E.; van Veggel, F. C. J. M.; Winnik, M. A., Determination of the Förster Distance in Polymer Films by Fluorescence Decay for Donor Dyes with a Nonexponential Decay Profile. *J. Phys. Chem. B* **2009,** *113*, 2262-2272.
73. Inal, S.; Kölsch, J. D.; Chiappisi, L.; Janietz, D.; Gradzielski, M.; Laschewsky, A.; Neher, D., Structure-related differences in the temperature regulated fluorescence response of LCST type polymers. *J. Mater. Chem. C* **2013,** *1*, 6603-6612.
74. Enzenberg, A.; Laschewsky, A.; Boeffel, C.; Wischerhoff, E., Influence of the Near Molecular Vicinity on the Temperature Regulated Fluorescence Response of Poly(N-vinylcaprolactam). *Polymers* **2016,** *8*, [109] 1-27.
75. Hildebrand, V.; Heydenreich, M.; Laschewsky, A.; Möller, H. M.; Müller-Buschbaum, P.; Papadakis, C. M.; Schanzenbach, D.; Wischerhoff, E., "Schizophrenic" self-assembly of dual thermoresponsive block copolymers bearing a zwitterionic and a non-ionic hydrophilic block. *Polymer* **2017,** *122*, 347-357.
76. Wattebled, L.; Laschewsky, A., New anionic gemini surfactant based on EDTA accessible by convenient synthesis. *Colloid Polym. Sci.* **2007,** *285*, 1387-1393.
77. Gradzielski, M.; Hoffmann, H.; Langevin, D., Solubilization of Decane into the Ternary System TDMAO/1-Hexanol/Water. *J. Phys. Chem.* **1995,** *99*, 12612-12623.
78. Flynn, J. H., Thermodynamic properties from differential scanning calorimetry by calorimetric methods. *Thermochim. Acta* **1974,** *8*, 69-81.
79. Wu, H., Correlations between the Rayleigh ratio and the wavelength for toluene and benzene. *Chem. Phys.* **2010,** *367*, 44-47.
80. Wohlfarth, C., Thermodynamic Properties: pVT-Data and Miscellaneous Properties of Polymer Solutions. In *Polymer Solutions: Physical Properties and their Relations I* Arndt, K.-F. L., M. D. eds., Ed. Springer: Berlin-Heidelberg (Germany), 2010.
81. Schnablegger, H.; Glatter, O., Simultaneous Determination of Size Distribution and Refractive Index of Colloidal Particles from Static Light-Scattering Experiments. *J. Colloid Interface Sci.* **1993,** *158*, 228-242.
82. Schnablegger, H.; Glatter, O., Optical sizing of small colloidal particles: an optimized regularization technique. *Appl. Opt.* **1991,** *30*, 4889-4896.
83. Bivigou-Koumba, A. M.; Kristen, J.; Laschewsky, A.; Müller-Buschbaum, P.; Papadakis, C. M., Synthesis of Symmetrical Triblock Copolymers of Styrene and N-isopropylacrylamide Using Bifunctional Bis(trithiocarbonate)s as RAFT Agents. *Macromol. Chem. Phys.* **2009,** *210*, 565-578.

84. Hildebrand, V.; Laschewsky, A.; Päch, M.; Müller-Buschbaum, P.; Papadakis, C. M., Effect of the Zwitterion Structure on the Thermo-responsive Behaviour of Poly(Sulfobetaine Methacrylate)s. *Polym. Chem.* **2017,** *8*, 310-322.
85. Ko, C.-H.; Henschel, C.; Meledam, G. P.; Schroer, M. A.; Müller-Buschbaum, P.; Laschewsky, A.; Papadakis, C. M., Self-Assembled Micelles from Thermoresponsive Poly(methyl methacrylate)-b-poly(N-isopropylacrylamide) Diblock Copolymers in Aqueous Solution. *Macromolecules* **2021,** *54*, 384-397.
86. Kujawa, P.; Aseyev, V.; Tenhu, H.; Winnik, F. M., Temperature-Sensitive Properties of Poly(N-isopropylacrylamide) Mesoglobules Formed in Dilute Aqueous Solutions Heated above Their Demixing Point. *Macromolecules* **2006,** *39*, 7686-7693.
87. Yamazaki, A.; Song, J. M.; Winnik, F. M.; Brash, J. L., Synthesis and Solution Properties of Fluorescently Labeled Amphiphilic (N-alkylacrylamide) Oligomers. *Macromolecules* **1998,** *31*, 109-115.
88. Kujawa, P.; Segui, F.; Shaban, S.; Diab, C.; Okada, Y.; Tanaka, F.; Winnik, F. M., Impact of End-Group Association and Main-Chain Hydration on the Thermosensitive Properties of Hydrophobically Modified Telechelic Poly(N-isopropylacrylamides) in Water. *Macromolecules* **2006,** *39*, 341-348.
89. Bivigou-Koumba, A. M.; Görnitz, E.; Laschewsky, A.; Müller-Buschbaum, P.; Papadakis, C. M., Thermoresponsive amphiphilic symmetrical triblock copolymers with a hydrophilic middle block made of poly(N-isopropylacrylamide): synthesis, self-organization, and hydrogel formation. *Colloid Polym. Sci.* **2010,** *288*, 499-517.
90. Fowler, M.; Duhamel, J.; Qiu, X. P.; Korchagina, E.; Winnik, F. M., Temperature response of aqueous solutions of pyrene end-labeled poly(N-isopropylacrylamide)s probed by steady-state and time-resolved fluorescence. *J. Polym. Sci., Part B: Polym. Phys.* **2018,** *56*, 308-318.
91. Ren, H.; Yang, P.; Winnik, F. M., Azopyridine: a smart photo- and chemo-responsive substituent for polymers and supramolecular assemblies. *Polym. Chem.* **2020,** *11*, 5955-5961.
92. Malfait, A.; Coumes, F.; Fournier, D.; Cooke, G.; Woisel, P., A water-soluble supramolecular polymeric dual sensor for temperature and pH with an associated direct visible readout. *Eur. Polym. J.* **2015,** *69*, 552–558.
93. Ren, H.; Qiu, X.-P.; Shi, Y.; Yang, P.; Winnik, F. M., Light, temperature, and pH control of aqueous azopyridine-terminated poly(N-isopropylacrylamide) solutions. *Polym. Chem.* **2019,** *10*, 5080-5086.
94. Ohnsorg, M. L.; Ting, J. M.; Jones, S. D.; Jung, S.; Bates, F. S.; Reineke, T. M., Tuning PNIPAm self-assembly and thermoresponse: roles of hydrophobic end-groups and hydrophilic comonomer. *Polym. Chem.* **2019,** *10*, 3469-3479.
95. Kirkland, S. E.; Hensarling, R. M.; McConaughy, S. D.; Guo, Y.; Jarrett, W. L.; McCormick, C. L., Thermoreversible Hydrogels from RAFT-Synthesized BAB Triblock Copolymers: Steps toward Biomimetic Matrices for Tissue Regeneration. *Biomacromolecules* **2008,** *9*, 481-486.
96. Škvarla, J.; Raya, R. K.; Uchman, M.; Zedník, J.; Procházka, K.; Garamus, V. M.; Meristoudi, A.; Pispas, S.; Štěpánek, M., Thermoresponsive behavior of poly(N-isopropylacrylamide)s with dodecyl and carboxyl terminal groups in aqueous solution: pH-dependent cloud point temperature. *Colloid Polym Sci.* **2017,** *295*, 1343-1349.

97. Lang, X.; Patrick, A. D.; Hammouda, B.; Hore, M. J. A., Chain terminal group leads to distinct thermoresponsive behaviors of linear PNIPAM and polymer analogs. *Polymer* **2018,** *145*, 137-147.

ToC Table of Content graphics